Interface Phonons in Semiconductor Heterostructures and Phonons in Molybdenum Di-

sulphide

BY

RAMJI SINGH
B.TECH., Uttar Pradesh Technical University, INDIA, 2005

THESIS

Submitted as partial fulfillment of the requirements
for the degree of Master of Science in Electrical and Computer Engineering
in the Graduate College of the
University of Illinois at Chicago, 2019

Chicago, Illinois

Defense Committee:

Michael A. Stroscio Chair and Advisor
Mitra Dutta
Inna Partin-Vaisband

ACKNOWLEDGEMENTS

Firstly, I am highly indebted to my advisor Dr. Michael A. Stroscio, who believed in me from the first day of research. His pioneering works in the field of phonons spurred immense curiosity in me. His office door was always open for me to clear my concepts and he worked with me, so I get a thorough understanding of the subject. He had been a strong support and my lighthouse who showed me the way to walk upon. Because of his guidance, in a very short period of time I was able to scale my understanding from basics to advance level.

I express my sincere gratitude to Dr. Mitra Dutta, whose works on optoelectronics and the role of phonons in this area which increased my curiosity to the next level to further understand this subject. Her guidance and informed discussions during our research group meeting had a very positive impact on me.

Many thanks to Dr. Inna Partin-Vaisband, under whom I learned to critically think and make logical deductions out of technical literature. I learned a lot about limitations of scaling transistors and methods to deal with it. I also learned how to intuitively think of the outcome of any analysis before it's mathematical treatment.

Finally, I express my gratitude to my parents and elder sisters for blessing me to pursue higher education at UIC and supporting me in all of my endeavors. I couldn't have walked a single step without them.

<div align="right">RS</div>

TABLE OF CONTENTS

iii

LIST OF TABLES

LIST OF FIGURES

LIST OF FIGURES (continued)

LIST OF ABBREVIATIONS

IF   Interface Phonon

Φ Fröhlich potential

m, M   Mass of different atoms

Q   Wave vector in isotropic plane

K   Phonon wave vector along c-axis

ω Frequency

$\hbar$ Reduced planck's constant

α Interatomic spring constant

$\varepsilon_{\parallel}$ Dielectric constant along c-axis

$\varepsilon_{\perp}$ Dielectric constant perpendicular to c-axis

$\text{erf}(x)$ Error function

SUMMARY

Interactions of electrons with longitudinal optical phonons (LO phonons) are the most dominant scattering mechanism in polar semiconductors. This interaction in polar semiconductors is known as the Fröhlich interaction and is the primary interaction determining the limiting electron mobility. In heterostructures, the confinement effects cause the LO phonons undergo significant modifications in terms of spectrum and the macroscopic fields produced by them; this leads to emergence of new modes.

This research introduces in-depth details about interface phonons (IF phonons) in two-interface wurtzite heterostructures and then advances the mathematical treatment to find the Fröhlich potential profile and spectrum for multi-interface wurtzite heterostructures. The knowledge of the electron interaction potential and the spectrum are fundamental to understand the electron scattering mechanism.

In the last part of this research, the profile of the potential is determined for 1-mono layer of molybdenum disulphide which is an emerging 2D material.

CHAPTER 1 INTRODUCTION

1.1 What are Phonons

The active materials finding application in the electronics industry are crystalline in nature. The constituent atoms of crystalline material are arranged periodically in three-dimensional arrays. However, in reality the atoms are not rigidly fixed in space inside the crystal, these atoms vibrate causing the interatomic spacing to vary periodically in time and space. The frequency of vibration increases with temperature. *The systematic and collective vibration of atoms possesses energy which is quantized; The quantum of energy is known as* **Phonons.**

In a bulk material there are the following types of phonons:

1. **Optical Phonons:** The constituent atoms of the crystals vibrate _out-of-phase_ with respect to each other. The figure below shows vibration pattern of atoms for optical phonon modes for a crystal with diatomic basis:
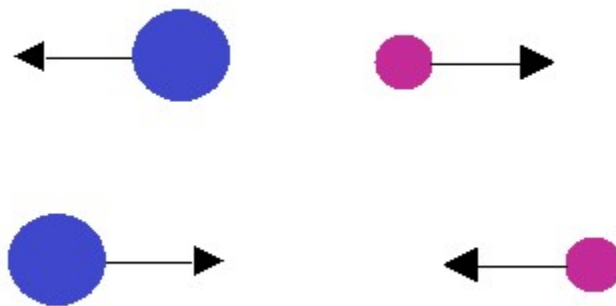
Figure 1 The vibration pattern of atoms for Longitudinal Optical phonon modes.

In the above figure the atoms vibrate along the same direction as that of the wave propagation; hence, these are termed as **Longitudinally Optical Phonons** abbreviated as LO Phonons. If the atoms vibrate perpendicular to the direction of the wave propagation, then they are referred to as **transverse optical phonons** abbreviated as TO phonons. It is to be noted that in polar semiconductors the two atoms as shown above are oppositely charged hence they produce macroscopic polarization field due to presence of phonons.

2. **Acoustic Phonons:** The constituent atoms of the crystals vibrate _in-phase_ with respect to each other. The figure below shows vibration pattern of atoms for acoustic phonon modes for a crystal with diatomic basis:
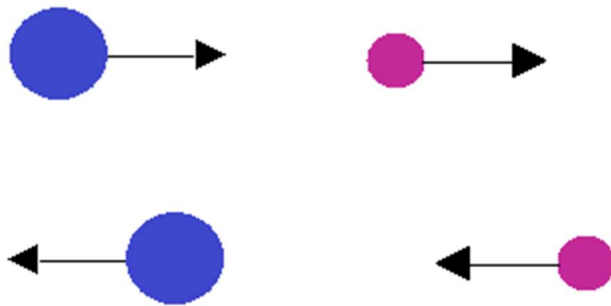
Figure 2 The vibration pattern of atoms for longitudinal acoustic phonon modes.

In the above figure the atoms vibrate along the same direction as that of the wave propagation; hence, these are referred to as **longitudinally acoustic phonons** abbreviated as LA phonons. If the atoms vibrate perpendicular to the direction of wave propagation, then they are termed as **transverse acoustic phonons**

abbreviated as TA phonons. It is to be noted that since the atoms vibrate in-phase with each other thus they do not produce polarization field unlike the optical phonon modes.

The relation between phonon the wavevector and the frequency is referred to as the **dispersion relation**. For bulk material this is derived using linear chain atomic model for a given dimension. It is frequently assumed that the two immediate atoms are tightly coupled to each other and the interaction between them is modelled using Hooke's law (This assumes that the restoring force between the atoms is directly proportional to the displacement over and above the equilibrium position). For a linear chain comprising of periodic placement of atoms as in Fig. 1 and 2, the dispersion relation for the longitudinal modes is given by [1]:

$$\omega^2 = \alpha\left(\frac{1}{m}+\frac{1}{M}\right) \pm \alpha\left[\left(\frac{1}{m}+\frac{1}{M}\right)^2 - \frac{4\,sin^2qa}{mM}\right]^{1/2}$$

The upper + sign is taken the case of the LO modes and the lower − sign is taken in the case of LA mode. The symbols in the above equations are:

$$m = mass\ of\ lighter\ atom\ in\ diatomic\ basis$$

$$M = mass\ of\ heavier\ atom\ in\ diatomic\ basis$$

$$\alpha = interatomic\ spring\ constant$$

$$q = phonon\ wavevector$$

$$\omega = phonon\ frequency$$

$$a = interatomic\ equillibrium\ spacing$$

The figure below shows the plot in the first Brillouin zone for frequency vs. wavevector relation for a diatomic basis crystal:
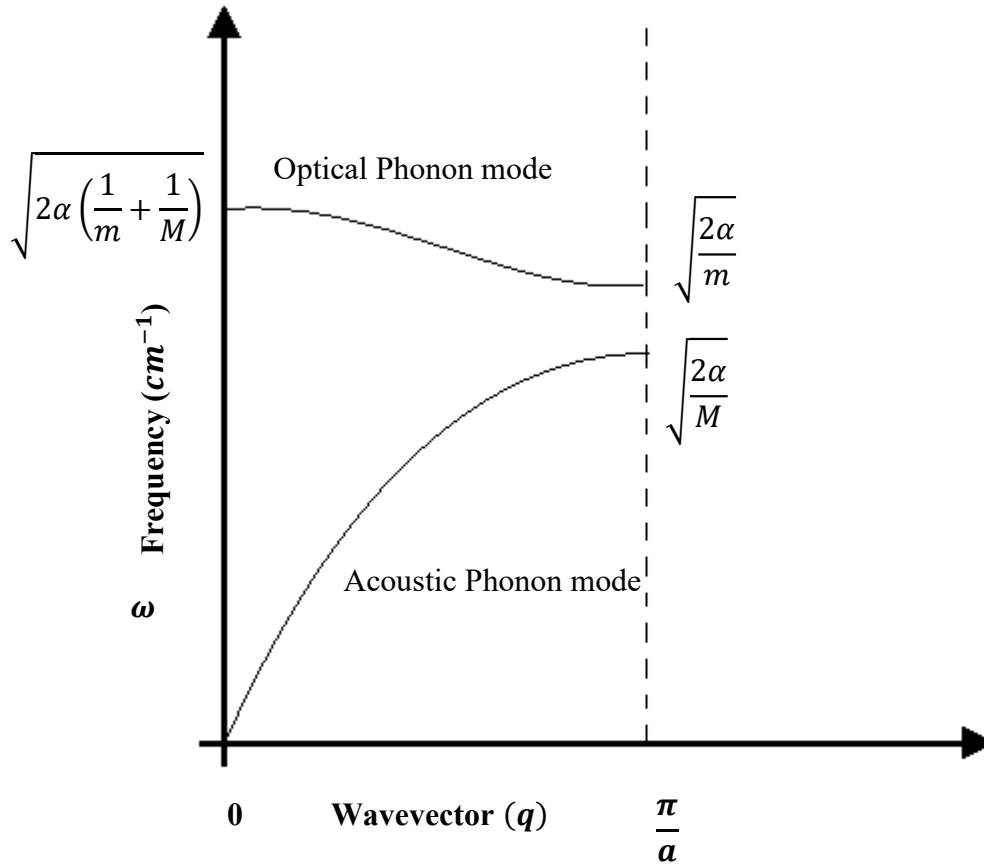
Figure 3 Dispersion relation of bulk phonons in a linear crystal with diatomic basis

The high frequency solution of Eq.1 yields the optical phonon modes whereas the low frequency solution yields the acoustic phonon modes.

The **group velocity (v_g)** is defined as the instantaneous slope of the curve in the dispersion relation, which is equal to, $\frac{d\omega}{dq}$. The group velocity represents the velocity of energy transmission in the material. It is evident that the acoustic modes have higher group velocity than the optical phonons near zone center (Γ-point) of the Brillouin zone.

1.2 Why are phonons important: Phonons give rise to numerous effects in semiconductors which significantly affect their electronic and optical properties; below are three significant phonon mediated effects in semiconductors which are essential for a thorough understanding of phonons:

1. **Dominant electron scattering mechanism:** The electron-phonon interaction is one of the fundamental interaction processes in solids that frequently provides the dominant scattering mechanism with exception being at low temperatures [3]. As pointed out earlier, the LO phonons in a polar semiconductor give rise to macroscopic polarization field which couples with the electron and results in energy exchange between the electron and LO phonon. An external electric field causes an electron to gain energy and hence accelerates it; however, when the electron energy reaches a threshold level (36 meV in GaAs and 91 meV in GaN), then the electron rapidly emits an LO phonon causing it to loose energy. Under steady state conditions, the energy gained from the external electric field is balanced by the energy lost by phonon emission, this eventually causes electron to move with a constant velocity also known as saturation velocity. This saturation velocity is the upper equilibrium limit on velocity of electron which it can attain inside a material. The acoustic phonon on the other hand causes the inter atomic distance between the atoms to fluctuate causing the conduction band energy levels to fluctuate accordingly, thus giving rise to a

deformation potential in the conduction band which interacts with the electron causing the loss of momentum and energy.

2. **Non-vertical transitions in indirect band gap semiconductors:** The density of electrons and holes in conduction and valence band respectively are maximum near the minima and maxima of conduction band and valence band as depicted in a typical **E-K** diagram. In an indirect band gap semiconductor the minima and maxima of conduction and valence band do not coincide. A photon when interacting with an electron can cause vertical transition to-from valence-conduction band transition, because the photon has very low momentum due low magnitude of wavevector since its wavelength is of the order of few hundreds of nanometers. Thus, the transitions caused by photon approximately preserves the momentum of electrons from its initial and final state, hence in an indirect semiconductor the probability of photon assisted transitions is very low. On the contrary, a phonon has energy much less than a photon but very high magnitude of wavevector (for example at the end of first Brillouin zone $k = \pi/2a$ where a = lattice constant and is of the order of few angstroms). Thus, emission-absorption of phonons can lead to phonon assisted transitions in indirect bandgap semiconductors.

3. **Exciton production-annihilation [2]:** Excitons are a hydrogen-atom like quasi-particle formed in semiconductors in which bound electron-hole pairs are present due to Coulomb interactions.

   The exciton energy levels are present inside the bandgap. A phonon with a high wavevector can produce an exciton; to conserve the momentum, the excitons, after formation, have high kinetic energies and can roam freely inside the crystal. Similarly, the phonons can

interact with excitons to annihilate by causing electron and hole to recombine. Understanding of exciton dynamics is very important for performance characterization of optoelectronic devices.

1.3 Emergence of new phonon modes in semiconductor quantum well

Komirenko et. al (1999) in landmark work applies Loudon's dielectric continuum model to uniaxial crystals study to various optical phonon modes in wurtzite-material-based quantum wells (QW). Uniaxial crystals have completely different electrical, optical and mechanical properties along a particular axis (c-axis), whereas the properties along the other two mutually perpendicular directions are the same. Because of this anisotropy, various effects such as lack of complete confinement of phonons in wurtzite quantum wells and the formation of finite energy intervals for confined modes occur in wurtzite QWs. Various new modes such as interface modes, half space modes and propagating modes appear in wurtzite QWs. The above modes have completely different frequency spectra than the bulk modes described earlier in the chapter.

1.4 Outline of Research Work:

The organization of research work presented in this thesis is as under: In Chapter 2, the first part we present the evaluation of analytical expressions and plots of graphs for dispersion relation and electron-phonon interaction potentials (also known as Frohlich potential) for interface modes in various two-interface wurtzite heterostructure terminated with semi-infinite layers. The second part deals with two heterostructures - (a) $Al_{1-x1}Ga_{x1}N/Al_{1-x2}Ga_{x2}N/Al_{1-x3}Ga_{x3}N$ (b) GaN/$In_xGa_{1-x}N$/GaN, in both of the heterostructures the range of x is found for which the

interface modes can exist as well as the corresponding range of frequency for which interface modes exist.

Chapter 3 presents the evaluation of analytical expressions for dispersion relations and interaction potentials for a two-interface metal-terminated wurtzite heterostructure. These heterostructures find application in dual gate MOSFETS. It is further discussed as to how metal terminations leads to reduced scattering of electrons by interface modes.

Chapter 4, presents a general theory based on the transfer matrix method for wurtzite heterostructure. This work is inspired by the work of Yu *et al.* (1997) which was developed for isotropic crystals. The theory so developed in Chapter 4 enables one to find dispersion relation and Frohlich potential for interface modes in any heterostructure consisting of an arbitrary number of layers. Further, the theory is applied to a 2-layer (AlN/GaN) 4-period superlattice to find the dipersion relation of interface modes.

Chapter 5, Analytical expressions are derived and graphs plotted for out-of-plane vibrations in 1-monolayer (1-ML) thick MoS_2. The recent available literature has treated only the in-plane vibration modes.

CHAPTER 2 Interface-Phonon — Electron Interaction Potentials and Dispersions Relations in III-Nitride-Based Structures

2.1. Introduction

The study of electron-optical-phonon interactions in semiconductor structures has been active for a variety of semiconductor heterostructures with particular emphasis on semiconductors based on cubic crystals [1]. In particular, the optical modes in such structures are known to facilitate fast phonon-assisted transitions for the case where the phonons are interface modes [4]. The Frohlich potentials and dispersion relations of joint optical phonon modes, known as interface optical phonons, have been shown to be derivable using transfer matrix techniques introduced by Yu et al. [5]. These techniques have been applied extensively for heterostructures based on cubic crystals as exemplified by Teng et al. [6]. Moreover, confined and interface modes on such heterostructures have been shown to be critical in the performance of semiconductor lasers [7,8]. Of special importance, such confined and interface phonon-assisted transitions have been shown to be important in the operation of quantum cascade lasers and it was shown that interface-phonon—assisted transitions can greatly enhance population inversions [9-11]. Of special interest to the present study of III-nitride structures with ternary layers, the dielectric continuum models of Lee et al. [12-13] and Komirenko et al. [14-15] provided formulations of models treating the confined and interface phonons in uniaxial crystals with wurtzite structures based on III-nitride materials being a representative material system. By extending out previous work [14-15], the work of Glieze et al. [16] provided an illuminating account of the interface phonon modes in special case of superlattices based on wurtzite superlattices. Other works on III-nitride structures,

Lin et al. [17] considered the mobility enhancements in AlGaN/GaN/SiC with stair-step and graded heterostructures and Gaska et al. [18] considered the high temperature performance of AlGaN/GaN high-electron-mobility field-effect transistors on SiC substrates. Subsequent works formulated the interface phonon modes for GaN-ZnO heterstructures [19] as well as the electron-phonon scattering rates in wurtzite structures [20]. Zhang et al. considered interface optical phonons in wurtzite quantum heterostructures with particular emphasis on SiC/GaN/vacuum and GaN/AlN/vacuum heterostructues. In the present work, we provide a generalized treatment of the formulation in Ref. 20, model the Frohlich interactions in more complex III-nitride based heterosctructures, and point out errors. Interface phonon modes of dual-gate metal-oxide-semiconductor field-effect transistors have been formulated in Ref. 22. Park et al. [23, 24] have recently investigated heat transport via interface modes that propagate before decaying into heat carrying acoustic phonons, electron mobility and saturation velocity limits in GaN-based structures with binary layers using the dielectric continuum model for uniaxial materials [3, 5, 20]; the generalization to interface modes in ternary-containing layers portends such application for an expanded class of nitride heterostructures. Herein, we derive expressions for the phonon-electron Frohlich interactions as well as the dispersion relations for these joint modes for the technologically important case of III-nitride ternary materials for a general value of the so-called "x-value" describing the composition of each ternary layer, such as $In_xGa_{1-x}N$, where x can have any specified value between 0 and 1.

There are four Sections in this chapter. In the following section, Section 2.2., we provide a generalize formulation of the Frohlich potentials and the dispersion relations of interface phonon modes in multi-layer heterostructures. Results and a discussion are presented in Section 2.3. Finally, Section 2.4. summarizes the conclusions of this paper.

2.2. Theory

The wurtzite structures considered in the paper have 4 atoms per unit cell and it follows that there are three acoustic modes and nine optical modes. Among the optical modes there are only two modes which couple strongly to electrons, so-called infrared active modes. The dielectric constants along the z-axis and perpendicular to the z-axis are given by:

$$\varepsilon_\perp(\omega) = \varepsilon_\perp^\infty \frac{\omega^2 - \omega_{\perp L}^2}{\omega^2 - \omega_\perp^2} \tag{1}$$

$$\varepsilon_z(\omega) = \varepsilon_z^\infty \frac{\omega^2 - \omega_{zL}^2}{\omega^2 - \omega_z^2} \tag{2}$$

where $\omega_{\perp L}$ and ω_{zL} represents the optical phonon frequencies of longitudinal modes along perpendicular to and parallel to z-axis and along z-direction, whereas, ω_z and ω_L are the optical frequencies of transverse modes. In the notation of the macroscopic dielectric continuum model, the classical electrostatic equations which are satisfied by the polar optical phonon fields [3, 12-15] are,

$$\vec{E}(\vec{r}) = -\nabla\Phi(\vec{r}) \tag{3}$$

$$\vec{D}(\vec{r}) = \vec{E}(\vec{r}) + 4\pi P(\vec{r}) = \varepsilon_\perp(\omega)E_\perp(\vec{r})\hat{\rho} + \varepsilon_z(\omega)E_z(\vec{r})\hat{z} \tag{4}$$

$$\nabla \cdot \vec{D}(\vec{r}) = 0 \tag{5}$$

where Φ is the potential introduced by the optical phonon modes, E represents electric field, D represents displacement field and P represents polarization field. Where, $\hat{\rho}$ and $\hat{z}$ represent the unit vectors perpendicular to and parallel to z- axis (which is also c-axis) respectively.

Substituting the equation for the electrostatic phonon potential $\Phi(r) = \Phi(z)e^{i\vec{q}\cdot\vec{\rho}}$ into Eq. 3, one finds

$$\nabla \cdot \vec{D} = \left(\varepsilon_z(\omega) \frac{\partial^2}{\partial z^2} - \varepsilon_\perp(\omega)q^2 \right) \Phi(\vec{r}) = 0 \tag{6}$$

Taking into account boundary conditions at $z = \pm\infty$, $\left. \Phi(z) \right|_{z \to \pm\infty} = 0$

It follows that for wurzite heterstructures as depicted in Fig. 4, that the phonon potential is:

$$\Phi(\vec{r}) = e^{i\vec{q}\cdot\vec{\rho}} \begin{cases} Ce^{k_1\left(z+\frac{d}{2}\right)} & z < -d/2 \\ A\cosh(k_2 z) + B\sinh(k_2 z) & -\frac{d}{2} \le z \le d/2 \\ De^{-k_3\left(z-\frac{d}{2}\right)} & z > d/2 \end{cases} \tag{7}$$

where A, B, C, and D are potential amplitudes in the various material regions and the wavevectors in the three regions are denoted by k_1, k_2 and k_3.

The intermediate layer has a thickness, d.

Applying the boundary conditions:

$$\tag{8}$$

$$\tag{9}$$

$$\Phi_i(z) = \Phi_{i+1}(z)$$

$$\varepsilon_i \frac{\partial \Phi_i}{\partial z} = \varepsilon_{i+1} \frac{\partial \Phi_{i+1}}{\partial z}$$

which express the facts that the normal component of D_z and the tangential component of $E_\perp$ are continuous at the interfaces. After eliminating the constants we get the secular equation of the system:

$$\frac{\varepsilon_{1z}k_1 + \varepsilon_{2z}k_2 \ tanh(k_2 d/2)}{\varepsilon_{2z}k_2 + \varepsilon_{1z}k_1 \ tanh(k_2 d/2)} = - \frac{\varepsilon_{3z}k_3 + \varepsilon_{2z}k_2 \ tanh(k_2 d/2)}{\varepsilon_{2z}k_2 + \varepsilon_{3z}k_3 \ tanh(k_2 d/2)} \qquad (10)$$

where $k = (k_z, q)$ is the phonon wave vector, such that

$$k_i = \sqrt{\frac{\varepsilon_{i,\perp}}{\varepsilon_{i,z}}} \ q \qquad (11)$$

with $\varepsilon_{i\perp}\varepsilon_{iz} > 0$ and i = 1, 2, 3 for the three regions of the heterostructure.

From the above dispersion relation the condition for symmetric and anti-symmetric Frohlich potentials can be derived separately. It is observed that for symmetric solution the dispersion relation will be:

$$\left(\varepsilon_{1z}k_1 + \varepsilon_{2z}k_2 \ tanh(k_2 d/2)\right)\left(\varepsilon_{3z}k_3 + \varepsilon_{2z}k_2 \ tanh(k_2 d/2)\right) = 0 \qquad (12)$$

Similarly, the condition for anti-symmetric potential will be:

$$\left(\varepsilon_{2z}k_2 + \varepsilon_{1z}k_1 \, tanh(k_2d/2)\right)\left(\varepsilon_{2z}k_2 + \varepsilon_{3z}k_3 \, tanh(k_2d/2)\right) = 0 \qquad (13)$$

Now, we can define the expression of potential separately as symmetric and anti-symmetric shown below:

$$\phi(r) = e^{i\vec{q}\cdot\vec{\rho}} \begin{cases} \phi_+ e^{k_1\left(z+\frac{d}{2}\right)} & ; z < -d/2 \\ \dfrac{\phi_+}{cosh\left(\frac{k_2d}{2}\right)} cosh(k_2z) & ; |z| < d/2 \\ \phi_+ e^{-k_3\left(z-\frac{d}{2}\right)} & ; z > d/2 \end{cases} \qquad (14)$$

The above is the expression for symmetric solution inside the quantum well. The anti-symmetric solutions will have the form shown below:

$$\phi(r) = e^{i\vec{q}\cdot\vec{\rho}} \begin{cases} -\phi_- e^{k_1\left(z+\frac{d}{2}\right)} & ; z < -d/2 \\ \dfrac{\phi_-}{sinh\left(\frac{k_2d}{2}\right)} sinh(k_2z) & ; |z| < d/2 \\ \phi_- e^{-k_3\left(z-\frac{d}{2}\right)} & ; z > d/2 \end{cases} \qquad (15)$$

Using the normalization condition for wurtzite material [3, 12-15]

$$\frac{\hbar}{2\omega L^2} = \sum \frac{1}{4\pi} \frac{1}{2\omega} \int_{R_i} dz \left(q^2 \frac{\partial \varepsilon_{i,\perp}(\omega)}{\partial \omega} |\Phi_i(q,z)|^2 + \frac{\partial \varepsilon_{i,z}(\omega)}{\partial \omega} \left| \frac{\partial \Phi_i(q,z)}{\partial z} \right|^2 \right) \qquad (16$$

and imposing the boundary conditions of Eqs.8 and Eqs. 9, it follows that:

The expression for symmetric solution

$$\Phi_+ = \sqrt{\frac{2h}{\varepsilon_0}} \left[\left(q^2 \frac{\partial \varepsilon_{11}}{\partial \omega} \frac{1}{2k_1} + \frac{\partial \varepsilon_{1z}}{\partial \omega} \frac{k_1^2}{2k_1} \right) + \left(q^2 \frac{\partial \varepsilon_{21}}{\partial \omega} \frac{1}{\cosh^2\left(\frac{k_2 d}{2}\right)} \left(\frac{d}{2} + \frac{si\quad(k_2 d)}{2k_2} \right) \right) + \right.$$

$$\qquad (17$$

$$\left. \frac{\partial \varepsilon_{2z}}{\partial \omega} \left(\frac{k_2^2}{co\quad^2\left(\frac{k_2 d}{2}\right)} \left(\frac{\sinh(k_2 d)}{2k_2} - \frac{d}{2} \right) \right) + \left(q^2 \frac{\partial \varepsilon_\perp}{\partial \omega} \frac{1}{2k_3} + \frac{\partial \varepsilon_z}{\partial \omega} \frac{k_3^2}{2k_3} \right) \right]^{-\frac{1}{2}}$$

and the expression for anti-symmetric solution is

$$\qquad (18$$

$$\phi_- = \sqrt{\frac{2h}{\varepsilon_0}} \left[\left(q^2 \frac{\partial \epsilon_{11}}{\partial \omega} \frac{1}{2k_1} + \frac{\partial \epsilon_{1z}}{\partial \omega} \frac{k_1^2}{2k_1} \right) \right.$$

$$+ \left(q^2 \frac{\partial \epsilon_{21}}{\partial \omega} \frac{1}{\sinh^2\left(\frac{k_2 d}{2}\right)} \left(\frac{\sinh(k_2 d)}{2k_2} - \frac{d}{2} \right) \right)$$

$$+ \frac{\partial \epsilon_{2z}}{\partial \omega} \left(\frac{k_2^2}{\sinh^2\left(\frac{k_2 d}{2}\right)} \left(\frac{\sinh(k_2 d)}{2k_2} + \frac{d}{2} \right) \right)$$

$$\left. + \left(q^2 \frac{\partial \epsilon_{31}}{\partial \omega} \frac{1}{2k_3} + \frac{\partial \epsilon_{3z}}{\partial \omega} \frac{k_3^2}{2k_3} \right) \right]^{-\frac{1}{2}}$$

2.3. Results and Discussion

The dispersion relations and Frohlich potential for the structure of Fig. 4 are depicted in Fig. 5 and Figs. 6 and 7, respectively. In GaN/In$_{0.15}$Ga$_{0.85}$N/GaN case the frequencies 720 cm^{-1} < ω < 735 cm^{-1} are the allowed rage of frequencies for IF phonon to exist in the entire heterostructure. The dispersion relations are based on Eq. 10 and the Frohlich potentials are based on Eqs. 20 and 21. In this example we illustrate the functional forms of the dispersion relations and the symmetric and anti-symmetric Frohlich potentials for the wurtzite heterostructure can be determined from Eq. 10 for the IF optical phonon modes.

For the heterostructure, with material 1 and 2, two cases are considered: SiC (6H)/GaN and GaN/AlN, respectively (as in Fig.5). Herein, the material 3 is taken as vacuum so we have ε_{3z} = $\varepsilon_{3\perp}$ = 1. Table 1 details parameters of every materials used in heterostructures under consideration.

For both SiC/GaN/Vacuum as well as GaN/AlN/Vacuum, we get four interface phonon modes- out of which two modes are symmetric and the other two modes are anti-symmetric in nature. For SiC/GaN/Vacuum heterostructure the allowed range of frequencies for Interface Phonon to exist in the structure is as below:

561 cm^{-1} < ω < 735 cm^{-1}

The dispersion curve for SiC/GaN/Vacuum heterostructure is shown in Fig. 9, whereas the symmetric Fröhlich potential graph is shown in Fig.10 and the anti-symmetric potential graph is shown in Fig.11. The Fröhlich potential graphs are drawn for qd = 3.

For GaN/AlN/Vacuum, the allowed range of frequencies is: 743 cm^{-1} < ω < 893 cm^{-1}

The dispersion curve for GaN/AlN/Vacuum heterostructure is shown in Fig. 12, whereas the symmetric Fröhlich potential graph is shown in Fig.13 and the anti-symmetric potential graph is shown in Fig.14. The Fröhlich potential graphs are drawn for qd = 3.

Importantly, the allowed interface modes must obey restrictive conditions on frequency which depend on the frequencies of the phonon modes in the layers composing the heterostructures. These frequency conditions are:

$$\varepsilon_{1z}(\omega)\varepsilon_{2z}(\omega) < 0 \ \& \ \varepsilon_{2z}(\omega)\varepsilon_{3z}(\omega) < 0 \ \& \ \varepsilon_{i,z}\varepsilon_{i,\perp}\big|_{i=1,2,3} > 0 \tag{19}$$

The above simultaneous condition leads to the conclusion that the heterostructure with compositions Al$_{0.15}$Ga$_{0.85}$N/Al$_{0.3}$Ga0$_{0.7}$N/Al$_{0.22}$Ga$_{0.78}$N does not have an allowed solution.

The following two sub-sections outlines detailed analysis for determining the range of composition labelled by x for existence of Interface modes in $\mathbf{Al_{1-x1}Ga_{x1}N/Al_{1-x2}Ga_{x2}N/Al_{1-x3}Ga_{x13}N}$ and $\mathbf{GaN/In_xGa_{1-x}N/GaN}$ heterostructures

1. Range of x for existence of Interface modes in $Al_{1-x1}Ga_{x1}N/Al_{1-x2}Ga_{x2}N/Al_{1-x3}Ga_{x13}N$ heterostructure

The procedure for determining the allowed frequency range of interface phonon modes in a three-layer heterostructure is illustrated for several different cases. The heterostructure under consideration comprises of a middle layer of $Al_{1-x2}Ga_{x2}N$ flanked by semi-infinite layers of $Al_{1-x1}Ga_{x1}N$ and $Al_{1-x3}Ga_{x3}N$ on left and right side respectively as shown in Fig. 15

Any heterostructure comprising wurtzite materials must obey the following two conditions simultaneously for the existence of interface phonon modes:

1. $\epsilon_{\parallel}\epsilon_{\perp} > 0$: In each individual layer, the product of dielectric constant along the c-axis or z-axis (which is the $\parallel$ direction here) and the dielectric constant along the direction perpendicular to c-axis (which is the $\perp$ direction here) must be greater than zero.

2. $\epsilon_{\parallel,i}\epsilon_{\parallel,i+1} < 0$: The product of dielectric constant along c-axis of two adjacent layers must be less than zero.

Table 3 shows optical phonon frequencies of $Al_{1-x}Ga_xN$ as a function of x.

Based on the data of Table 3, Fig.16 illustrates the range of frequencies for which $\epsilon_{\parallel}\epsilon_{\perp} > 0$ and the sign of $\epsilon_{\parallel}$ which is true for all values of x. The shaded portion in Fig. 16 represents frequency range for which $\epsilon_{\parallel}\epsilon_{\perp} > 0$

Similarly, the shaded portion in Figure 17 shows the range of frequency for which $\epsilon_{\parallel}$ is positive and the unshaded portion shows the range for which it is negative.

Based on the two essential conditions for interface phonons and the above two figures showing the ranges for the dielectric constant expressions, the categories of heterostructures supporting interface phonon modes in all three **Al$_{1-x}$ Ga$_x$ N** layers follow:

Type A: In this heterostructure the $\epsilon_{\parallel}$ of individual layers will alternate as: -/+/-

Type B: In this heterostructure the $\epsilon_{\parallel}$ of individual layers will alternate as: +/-/+

For the Type A heterostructure the following two structures exist:

First Case: It is noted that $\epsilon_{\parallel} < 0$ for $\omega_z < \omega < \omega_{zL}$, thus for simplicity we will omit the diagrams of $\epsilon_{\parallel}$ (as in Fig. 17) and use the frequency range diagrams for $\epsilon_{\parallel}\epsilon_{\perp}$ (as in Fig. 16) for Layer1 , 2 & 3 in that order for better understanding as shown in Fig. 18.

The condition depicted in Fig. 18 is possible only when $\omega_{z2} > \omega_{\perp 1}$ and $\omega_{z2} > \omega_{\perp 3}$, whereas, the range of interface phonon frequency is ω_{z2} - $\omega_{\perp 1}$ or ω_{z2} - $\omega_{\perp 3}$ depending on $\omega_{\perp 1}$ is greater than $\omega_{\perp 3}$ or lesser than $\omega_{\perp 3}$ respectively. Fig. 18 shows an example where $\omega_{\perp 1} < \omega_{\perp 3}$.

For example, this is achieved if $0 < x_1 < 0.2$ then $0.78 < x_2 < 1$; this opens the window : ω_{z2} - $\omega_{\perp 1}$, also, from Table. 3 data it is observed that an increase in x causes increase in $\omega_{\perp}$, thus the

choice of x_3 depends on how much narrower the range of allowed frequency is required for phonons, if x_3 is chosen such that $x_3 \geq x_1$ then it will further restrict the range of allowed frequency to ω_{z2} - $\omega_{\perp 3}$. Since a further increase in x_3 would constrict more the ω_{z2} - $\omega_{\perp 3}$ window, so the maximum value of x_3 should be identified based on the desired frequency range.

If x1 is increased beyond 0.2 then the range of x_2 is shown in Table 4.

If $x_3 \leq x_1$ then $\omega_{\perp 3} \leq \omega_{\perp 1}$ the range of interface modes is: ω_{z2} - $\omega_{\perp 1}$ and if $x_3 > x_1$ then the range is: ω_{z2} - $\omega_{\perp 3}$ in this case the care must be taken to not to increase x_3 so much so that $\omega_{\perp 3} \geq \omega_{z2}$.

Second Case:

Fig. 19 depicts the case of Type A heterostructure for the Second Case. In this case, the interface modes can exist in the heterostructure if $\omega_{\perp L2} < \omega_{zL1}$ and $\omega_{\perp L2} < \omega_{zL3}$.

The range of interface mode is: ω_{zL} - $\omega_{\perp L2}$ or ω_{zL} - $\omega_{\perp L2}$ depending on whether ω_{zL3} is greater or less than ω_{zL1}. Fig. 19 shows the case for $\omega_{zL} < \omega_{zL1}$.

Table 3 shows variation of optical phonon frequencies with x it can be concluded that, if, $0 < x_1 < 0.37$ then $0.5 < x_2 < 1$. The choice of x_3 depends on the range of interface modes required, if ω_{zL} - $\omega_{\perp L2}$ is the required range then $x_3 \leq x_1$, whereas if ω_{zL} - $\omega_{\perp L2}$ is the required range then $x_3 > x_1$ but in this case the upper limit on increase of x_3 should be such that $\omega_{\perp L2} < \omega_{zL}$.

For all x_1 in the range, $0.37 < x_1 < 0.7$ then $x_2 \geq x_1 + 0.13$, the choice of x_3 should be done as in the preceding paragraph.

For all x_1 in the range, $0.7 < x_1 < 0.85$ then $x_2 \geq x_1 + 0.08$, the choice of x_3 should be done as in the preceding paragraph.

For all x_1 in the range, $0.85 < x_1 < 1$ then $x_2 > x_1$, the choice of x_3 should be made as in the preceding paragraph.

For the Type B heterostructure the following two structures exist:

First case:

Fig. 20 depicts the case of Type B heterostructure for the First Case. In this case, the Interface modes can exist in the heterostructure if: $\omega_{\perp 2} < \omega_{z3} < \omega_{z1}$ in this case the range of Interface modes will be: $\omega_{z3} - \omega_{\perp 2}$, this corresponds to $x_3 > x_1$. The second case for existence is $\omega_{\perp 2} < \omega_{z1} < \omega_{z3}$ in this case the range of Interface modes will be: $\omega_{z1} - \omega_{\perp 2}$, this corresponds to $x_3 < x_1$.

This case is similar to the First case of Type A heterostructure with layer 1 and 2 interchanged, so the same limitations on x_1 and x_2 will apply as in Type A case. The choice of x_3 as indicated above can be made depending on the range of required frequency range.

Second Case:

Fig. 20 depicts the case of Type B heterostructure for the First Case. In this case, the Interface modes can exist in the heterostructure if : $\omega_{\perp L1} < \omega_{\perp L3} < \omega_{zL2}$ in this case the range of Interface modes will be: $\omega_{zL2} - \omega_{\perp L3}$, this corresponds to the case for $x_3 < x_1$. The second case for existence of interface mode is: $\omega_{\perp L3} < \omega_{\perp L1} < \omega_{zL}$ in this case the range of interface modes will be: $\omega_{zL} - \omega_{\perp L1}$, this case corresponds to the case of $x_3 > x_1$.

This case is similar to the Type A second case, thus, the restriction on x_1 and x_2 will be same as in Type A second case. The choice of x_3 as indicated previously can be made depending on the range of desired frequency range.

2 . Range of x for existence of Interface modes in GaN/In$_x$Ga$_{1-x}$N/GaN heterostructure

Consider the case of the heterostructure with a middle In$_x$Ga$_{1-x}$N layer flanked by GaN layer on both the sides. The shaded region in the below graphs show the range of frequencies for which $\epsilon_\parallel \epsilon_\perp \geq 0$ and $\epsilon_\parallel > 0$ in GaN respectively: The shaded portion in Fig.22 represents frequency range for which $\epsilon_\parallel \epsilon_\perp > 0$ for GaN

Similarly, the shaded portion in Fig. 23 shows the range of frequency for which $\epsilon_\parallel$ is positive and the unshaded portion shows the range for which it is negative for GaN.

The variation of optical phonon frequencies for $In_x Ga_{1-x}N$ with respect to x is shown in Table. 5.

Let us explore the possibility of existence of four different possible heterostructure for a 3- layer case of GaN/ $In_x Ga_{1-x}N$ /GaN. This case corresponds to $x_1 = x_3 = 0$. The following paragraphs discuss all four heterostructures:

Type A First Case: This case requires condition $\omega_\perp(GaN) < \omega_z(In_x Ga_{1-x}N) < \omega_{zL}(GaN)$ as shown in Fig. 24.

From the Table 5, on phonon frequencies for $In_x Ga_{1-x}N$ vs. x, it is observed that, for no value of x $\omega_z > 559\ cm^{-1}$, rather ω_z decreases with increase in x. The highest value of $\omega_z = 531\ cm^{-1}$ for $x = 0$. Thus, it is concluded that this possible combination of heterostructure cannot exist.

Type A Second Case: This case requires condition $\omega_\perp(GaN) < \omega_{\perp L}(In_x Ga_{1-x}N) < \omega_{zL}(GaN)$ as shown in Fig. 25

From the Table 5, on phonon frequencies for $In_x Ga_{1-x}N$ vs. x, it is observed that, for $0.07 \leq x < 1$, $\omega_{\perp L} \leq 734\ cm^{-1}$. As evident from the figure above the range of interface mode will be $\omega_{zL}(GaN) - \omega_{\perp L}(In_x Ga_{1-x}N)$.

Type B First Case: For GaN, the $\omega_z = 531\ cm^{-1}$; thus, for the interface modes to exist in this type of heterostructure only those value of x for $In_x Ga_{1-x}N$ layer are allowed such that: $\omega_\perp(In_x Ga_{1-x}N) \leq$

ω_z(GaN). And the range of allowed frequency for interface mode is: ω_z(GaN) $-\omega_\perp$(In$_x$Ga$_{1-x}$N), Fig. 26 shows the present case and the relevant frequency for interface mode existence.

From the Table 5, on phonon frequencies for In$_x$Ga$_{1-x}$N vs. x, it is observed that if $0.35 \leq x < 1$ then the above condition is satisfied. Hence, the allowed frequency range for interface modes is $531\ cm^{-1} - \omega_\perp(In_xGa_{1-x}N)$.

Type B Second Case: Fig. 27 shows the range of frequencies for existence of interface modes. For this combination the constraint imposed is $\omega_{zL}(In_xGa_{1-x}N) > 741\ cm^{-1}$. The table of phonon frequencies for In$_x$Ga$_{1-x}$N Vs x shows that $\omega_{zL}(In_xGa_{1-x}N)$ is never greater than $741\ cm^{-1}$ for any value of x. Thus, it can be concluded that no interface modes can exist in this heterostructure for frequencies greater than $741\ cm^{-1}$.

The Table 6 summarizes the maximum possible range vis-à-vis the range of x for all four combinations of heterostructures for GaN/$In_xGa_{1-x}N$/GaN.

2.4. Conclusion

This chapter derives general expressions for the dispersion relations and interface potentials for the joint interface optical phonon modes in uni-axial crystals exemplifies by ternary-based nitride heterostructures such as those illustrated for the specific cases of the symmetric heterostructure: GaN/In$_{0.15}$Ga$_{0.85}$N/GaN heterostructure (as a representative case of a ternary layer), as well as two asymmetric heterostructures: SiC/GaN/Vacuum and AlN/GaN/Vacuum. Interestingly, the allowed interface modes must obey restrictive conditions on frequency which depend on the

frequencies of the phonon modes in the layers composing the heterostructures. For example, application of the frequency conditions discussed in Section III. indicate that the heterostructure with compositions $Al_{0.15}Ga_{0.85}N/Al_{0.3}Ga0_{0.7}N/Al_{0.22}Ga_{0.78}N$ does not have an allowed solution. Although it is beyond the scope of the present paper, it is worth pointing out the potential application of our formalism to structures containing van der Waals layers. Consider the case of MoS_2 grown on GaN; this case is equivalent to a two-interface heterostructure with layers: MoS_2/Vacuum/GaN. The vacuum layer in the middle is due to van der Waals gap. For MoS_2 it is observed that $A_{2L}^{''} \ (\omega_{zL}) = A_{2T}^{''} \ (\omega_z) = 473 \ cm^{-1}$ due to which the dielectric constant along the z direction (perpendicular to interface), $\epsilon_{\parallel} > 0$ at all frequencies. Also, the middle vacuum layer, which is isotropic medium, the dielectric constant in all directions is equal to 1. From above, $\epsilon_{\parallel,vac}(\omega) = 1$ and $\epsilon_{\parallel,MoS2}(\omega) > 0$, thus, it is concluded that $\epsilon_{\parallel,vac}\epsilon_{\parallel,MoS2} \nless 0$ for any frequency which makes existence of joint interface phonon impossible. Of course, there can be evanescent tails of the Frohlich potentials on the vacuum region from the two layers surrounding the vacuum layer, but the evanescent potentials do not form joint interface modes for the entire material structure.

Tables

	$\omega_{zL}(cm^{-1})$	$\omega_{\perp L}(cm^{-1})$	$\omega_z(cm^{-1})$	$\omega_\perp(cm^{-1})$	ε^∞
$In_{0.15}Ga_{0.85}N$	715	720	525	550	5.76
GaN[26]	734	743	531	559	5.29
AlN[27]	893	916	660	673	4.68
SiC	964	970	788	797	6.61

Table I Material parameters of AlN, SiC , GaN and In0.15Ga0.85N.

	Frequencies	$\Phi_+ L$	$\Phi_- L$
SiC/GaN/Vac (for qd =1)	590.05 (Symmetric)	8.92	-
	694 (Symmetric)	21.61	-
	629 (anti-symmetric)	-	11.43
	721.66 (anti-symmetric)	-	14.65
GaN/AlN/Vac (for qd =3)	836.6 (Symmetric)	17.32	-
	864.9 (Symmetric)	19.81	-
	840 (anti-symmetric)	-	16.62
	866.7 (anti-symmetric)	-	18.95
$GaN/In_{0.15}Ga_{0.85}N/GaN$ (for qd =1)	731.8 (Symmetric)	27.84	-
	722.8 (anti-symmetric)	-	20.42

Table II Coefficients of Frohlich potential in various Heterostructures

X	ω_Z	$\omega_\perp$	ω_{ZL}	$\omega_{\perp L}$
0.05	607.72	667.01	883.51	905.41
0.1	604.89	662.87	875.48	898.71
0.15	602.05	660.05	872.69	892.01
0.2	600.51	657.21	864.65	886.59
0.25	597.67	653.08	860.58	879.89
0.3	594.84	648.96	853.88	873.18
0.35	592.01	644.84	847.16	866.48
0.4	589.16	639.43	840.46	858.49
0.45	586.34	636.59	833.76	850.51
0.5	583.49	631.18	825.78	842.52
0.55	580.66	627.06	820.37	835.82
0.6	579.11	622.93	812.38	827.83
0.65	573.71	617.52	804.39	818.55
0.7	569.58	612.11	796.4	809.27
0.75	565.45	605.4	787.12	800
0.8	561.34	599.99	777.83	789.42
0.85	555.92	592	768.56	777.57
0.9	550.51	584.01	757.98	767
0.95	542.52	573.45	747.43	753.86

Table III Optical phonon frequencies of $Al_{1-x}Ga_xN$ vs. x

data based on Fig. 1 of SeGi Yu et al, PRB, 58, 15,283 (1998) [Ref 34]

x_1	x_2
0.2 – 0.3	0.83 - 1
0.3- 0.4	0.86 - 1
0.4 – 0.5	0.88 -1
0.5 -0.6	0.97-1

Table IV Range of x_2 when $x_1 > 0.2$

29

X	ω_Z	$\omega_\perp$	ω_{ZL}	$\omega_{\perp L}$
0.05	529.58	554.93	726.76	735.21
0.1	523.94	550.7	721.13	726.76
0.15	519.72	546.48	714.08	719.72
0.2	515.49	543.66	707.04	712.68
0.25	511.27	539.44	700	705.63
0.3	505.63	535.21	692.96	698.59
0.35	502.82	532.39	685.92	690.14
0.4	497.18	525.35	678.87	682.39
0.45	492.96	522.54	670.42	676.06
0.5	488.73	518.31	663.38	669.01
0.55	484.51	514.08	653.52	660.56
0.6	478.87	508.45	646.48	653.52
0.65	476.06	505.63	638.03	643.66
0.7	471.13	501.41	630.99	635.21
0.75	467.61	498.59	623.94	626.76
0.8	463.38	492.96	612.68	615.49
0.85	457.75	488.73	604.23	605.63
0.9	454.93	483.1	594.37	597.18
0.95	449.3	480.28	583.1	585.92

Table V Optical phonon frequencies for $In_x Ga_{1-x} N$ Vs x

data based on Fig. 1 of SeGi Yu et al, PRB, 58, 15,283 (1998) [Ref 34]

Heterostructure Type	Range of x	Allowed frequency range
Type A First Case	No Solution	Cannot exist
Type A Second Case	0.07 -1	574 - 734
Type B First Case	0.37 - 1	475 - 531
Type B Second Case	No Solution	Cannot Exist

Table VI Summary of the maximum possible range vis-à-vis the range of x for all four combinations of heterostructures for GaN/$In_xGa_{1-x}N$ /GaN.

Figures
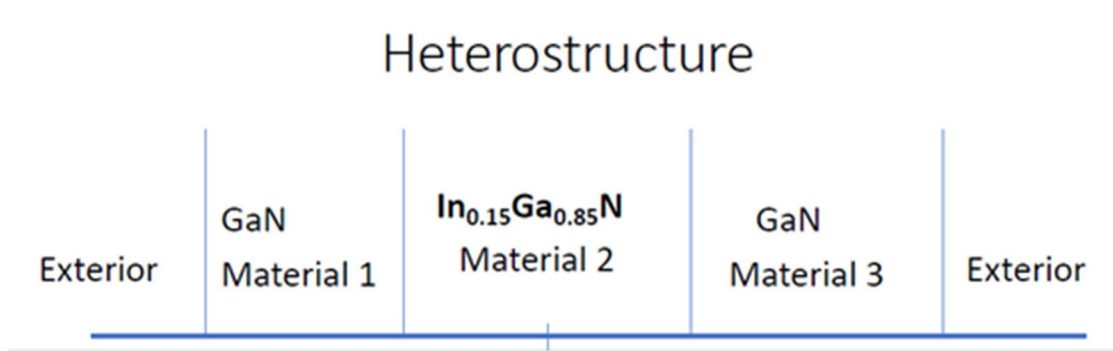
Figure 4 GaN-InGaN-GaN heterostructure used an example of applying the generalized Frohlich potentials and dispersion relations derived herein.
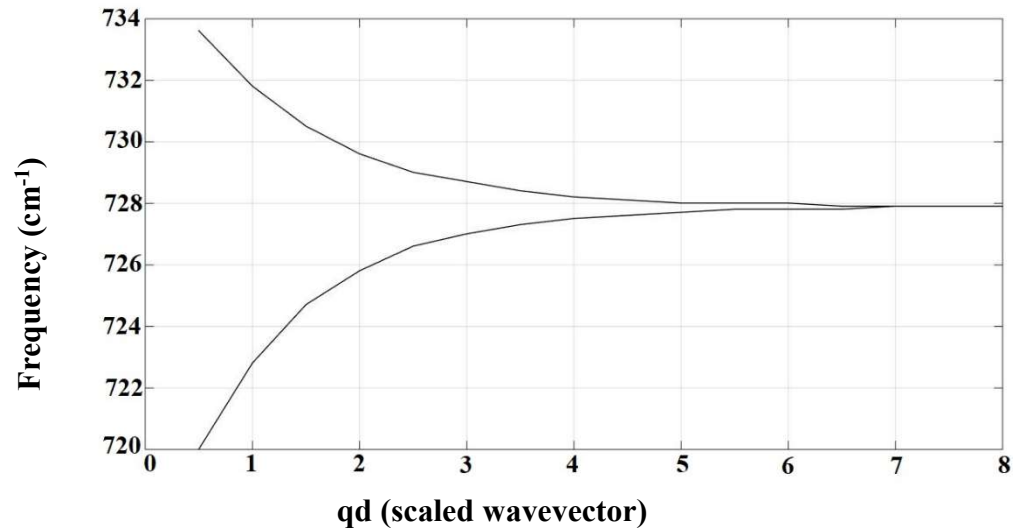
Figure 5 Dispersion curves interface modes of GaN/In0.15Ga0.85 N/GaN structure.
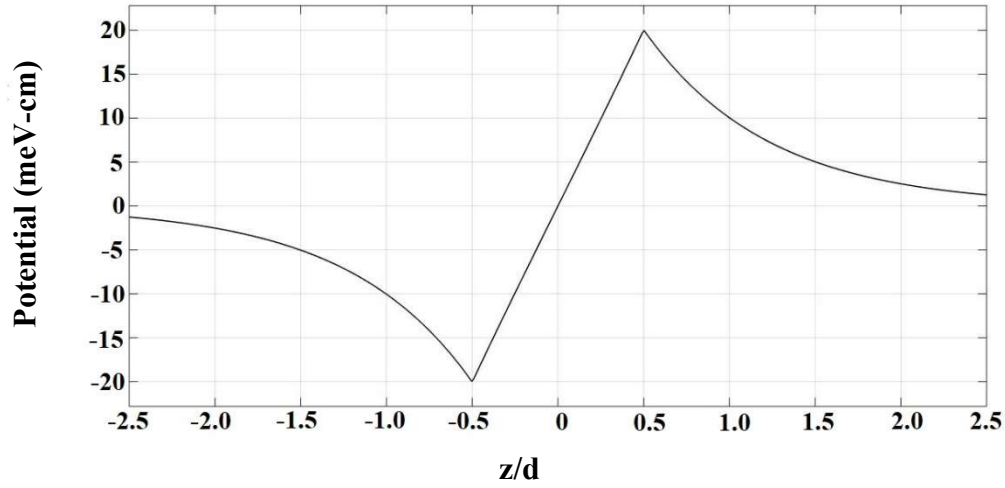
Figure 6 Anti-symmetric Frohlich potential for GaN/In0.15Ga0.85 N/GaN structure; qd = 1.
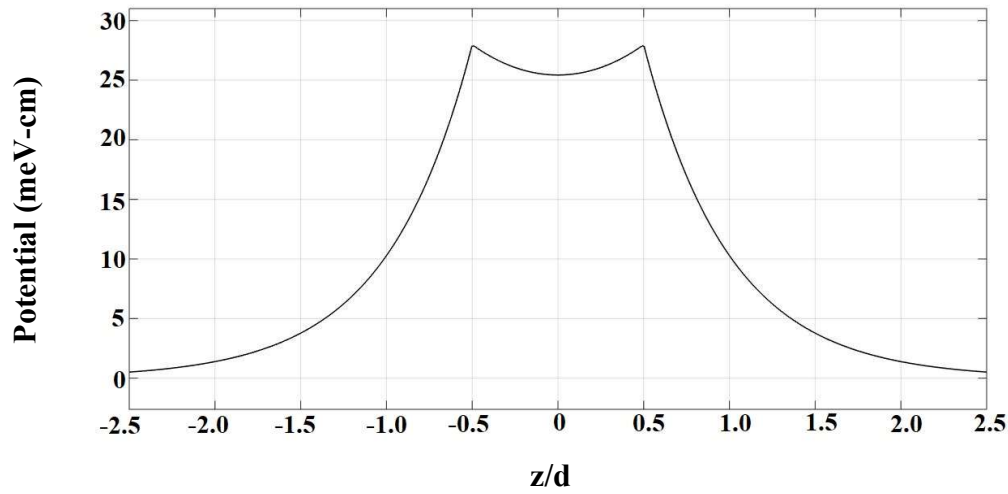
Figure 7 Symmetric Frohlich potential for GaN/In0.15Ga0.85 N/GaN structure; qd = 1.
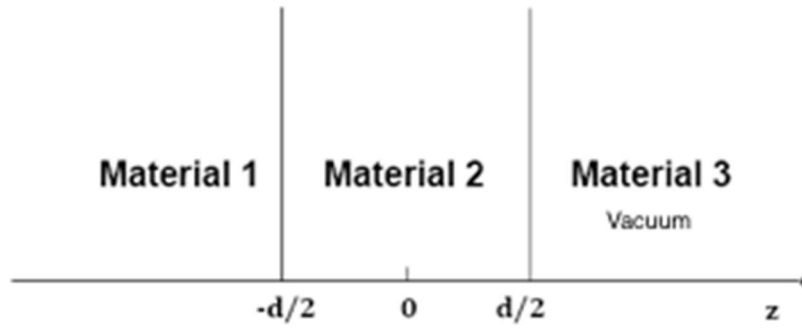
Figure 8 The two-interface heterostructure

qd (scaled wavevector)
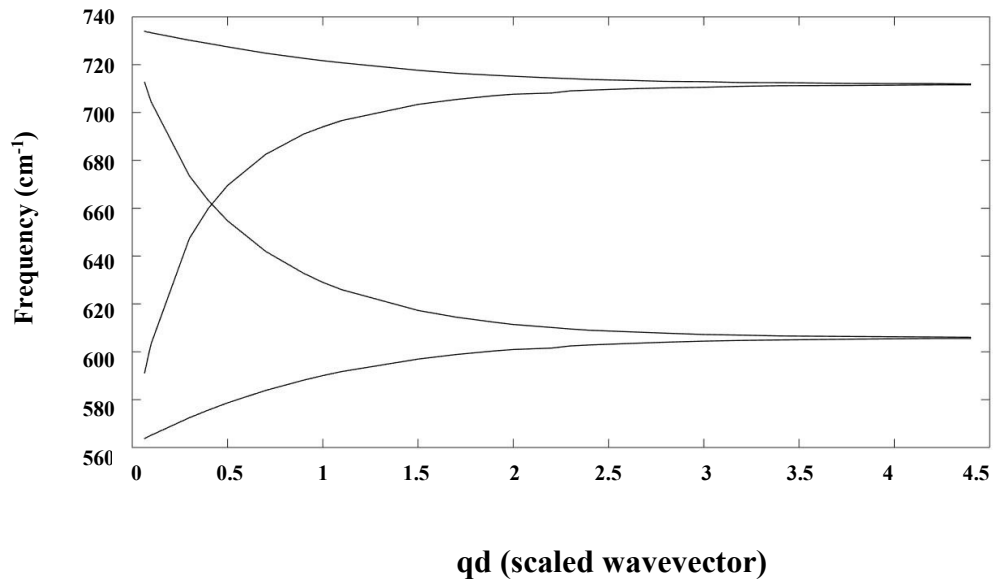
Figure 9 Dispersion curve for SiC/GaN/Vacuum
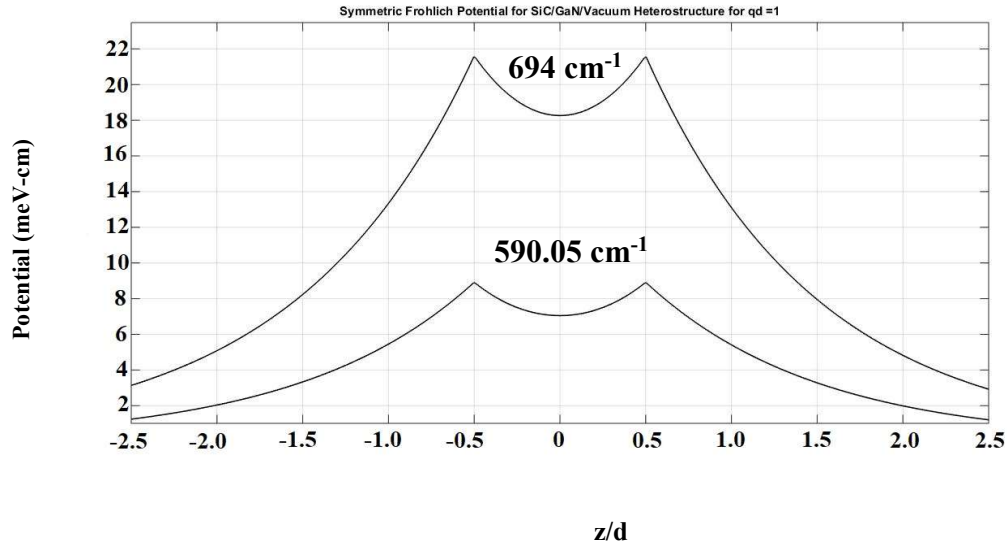
Figure 10 Symmetric Frohlich potential graph for qd =1, SiC/GaN/Vac
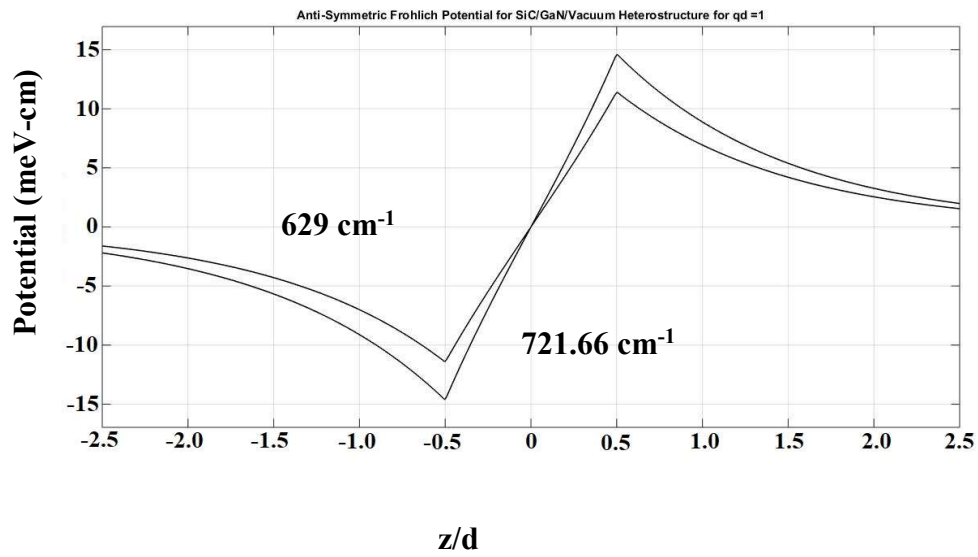
Figure 11 Anti-symmetric Frohlich potential graph for qd =1, SiC/GaN/Vac
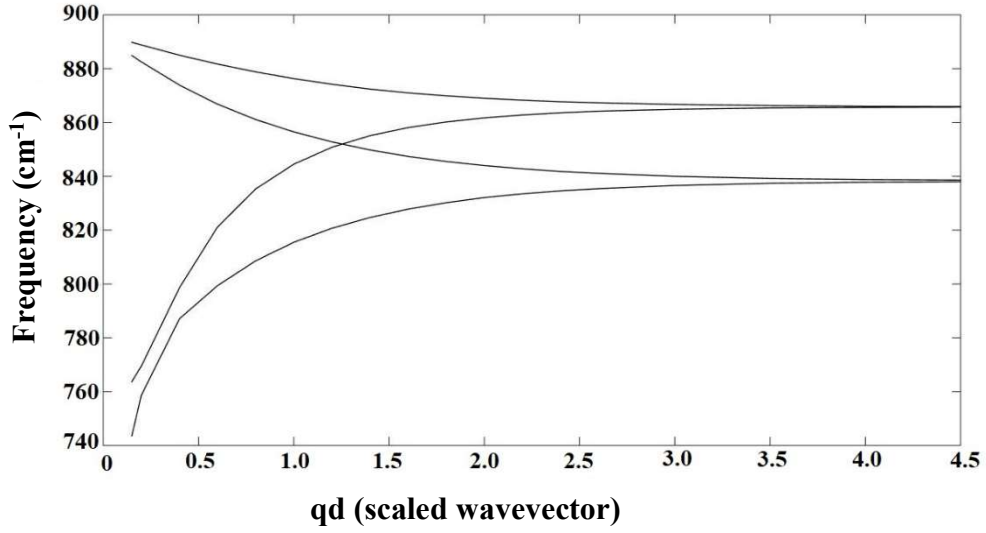
Figure 12 Dispersion curve for GaN/AlN/Vacuum
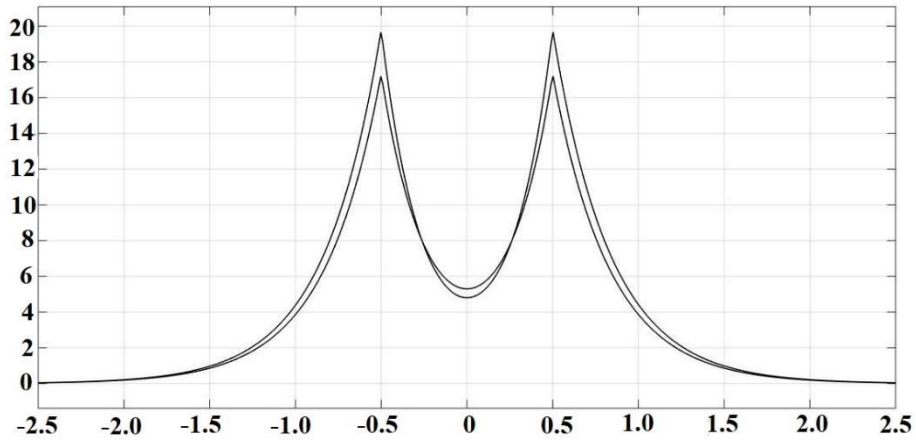
Figure 13 Symmetric Frohlich potential graph for qd =3, GaN/AlN/Vacuum
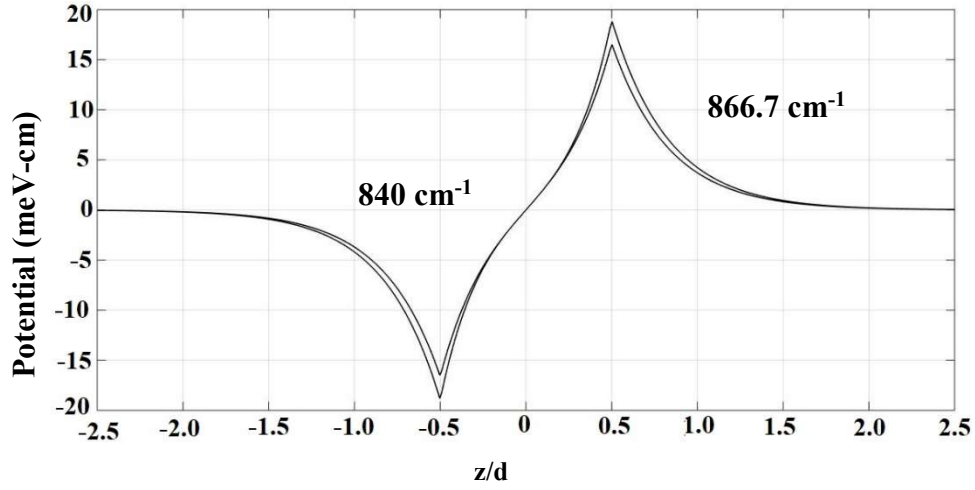
Figure 14 Anti-symmetric Frohlich potential graph for qd =3, GaN/AlN/Vacuum
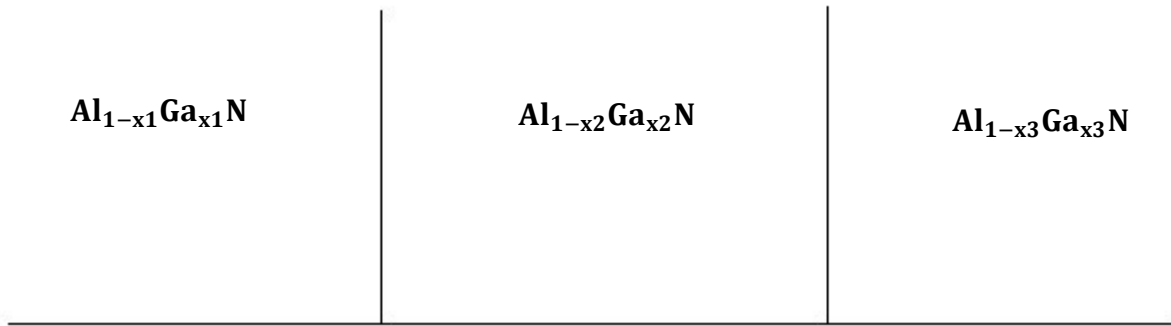
Figure 15 Two-interface heterostructure with semi-infinite end layers.

Figure 16 Shaded region showing the range of frequencies for which $\varepsilon_{\parallel}\varepsilon_{\perp} > 0$.

Figure 17 Shaded region showing the range of frequencies for which $\varepsilon_{\parallel} > 0$.

Range: $\omega_{z2} - \omega_{\perp 3}$
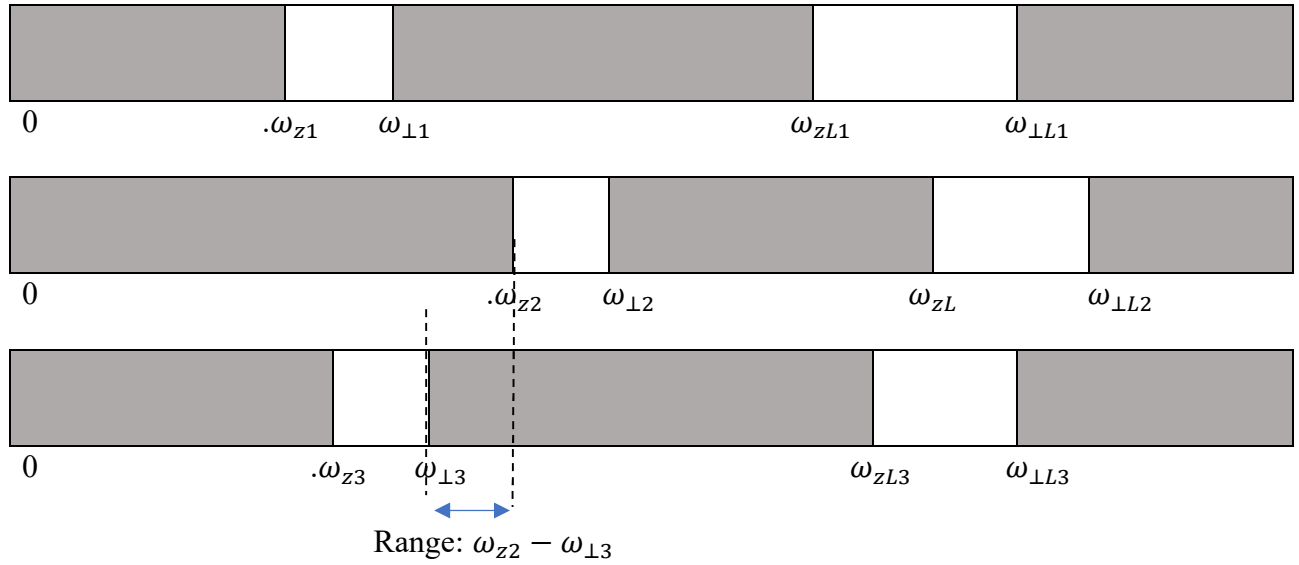
Figure 18 Type A: First Case.

The arrangement of 3 layers of a heterostructure for Type A First case with $\omega_{\perp 1} < \omega_{\perp 3} < \omega_{z2}$; the region of allowed frequencies is shown by the bar with double arrows.

Range = $\omega_{zL3} - \omega_{\perp L2}$
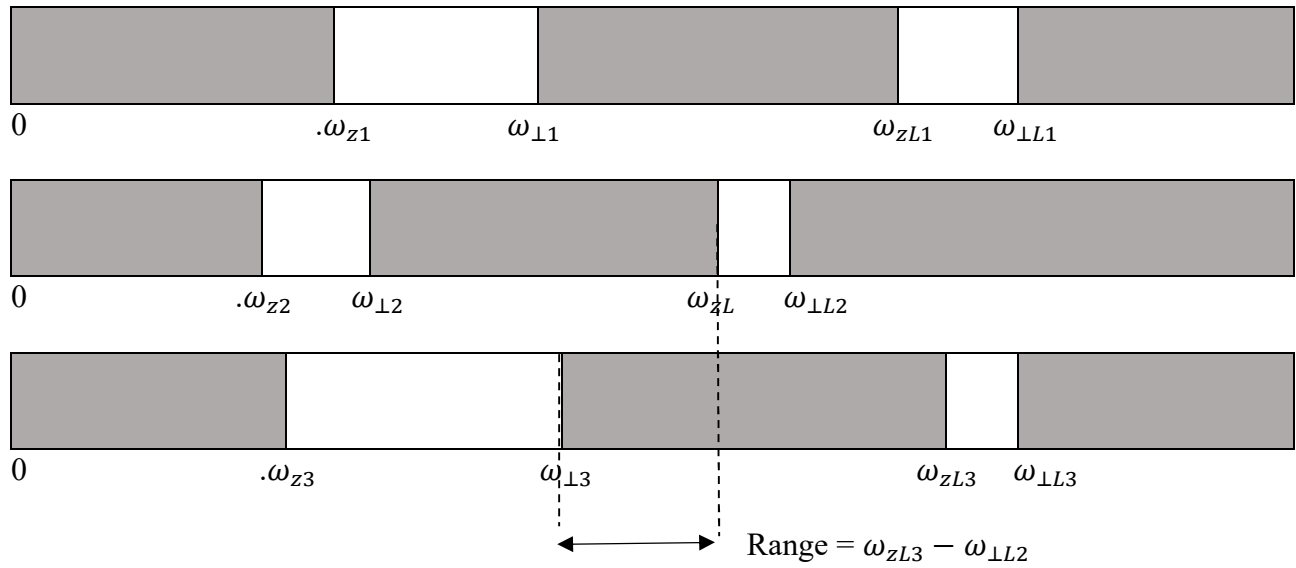
Figure 19 Type A: Second Case

The arrangement of 3 layers of heterostructure for Type A Second case with $\omega_{\perp 2} < \omega_{zL1} < \omega_{zL3}$. It is to be noted that $\omega_{zL} < \omega_{zL3}$ or $\omega_{zL} > \omega_{zL}$, these relationships only affect the range of allowed frequency; the region of allowed frequencies is shown by the bar with double arrows.

Range: $\omega_{z3} - \omega_{\perp 2}$
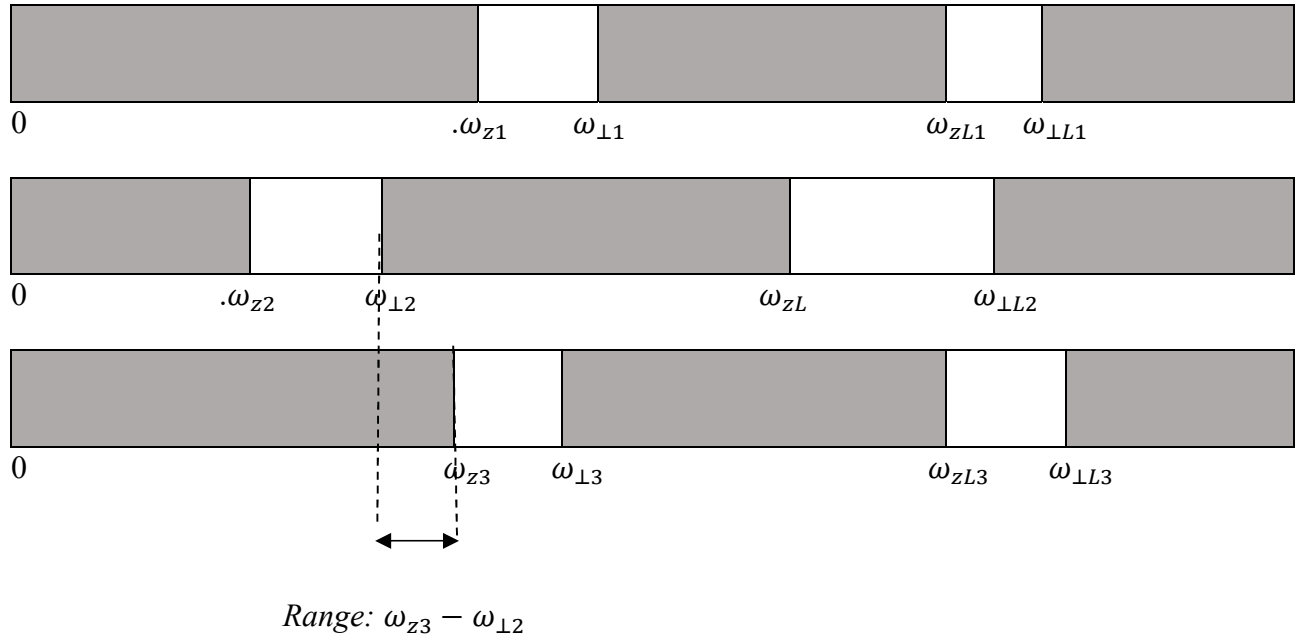
Figure 20 Type B: First Case

The arrangement of 3 layers of heterostructure for Type B First case with $\omega_{\perp 2} < \omega_{z3} < \omega_{z1}$. The relation between ω_{z1} and ω_{z3} only affects the range of allowed frequency t; the region of allowed frequencies is shown by the bar with double arrows.

Range: $\omega_{zL2} - \omega_{\perp L3}$
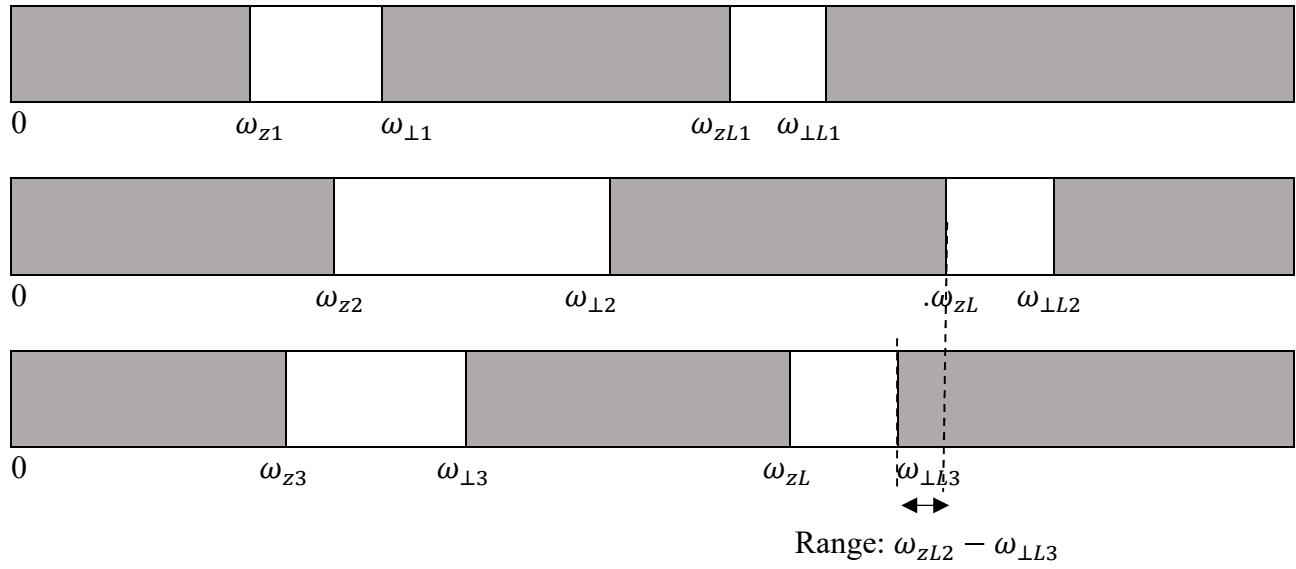
Figure 21 Type B: Second Case

The arrangement of 3 layers of a heterostructure for Type B Second case with $\omega_{\perp L1} < \omega_{\perp 3} < \omega_{zL2}$. The relation between $\omega_{\perp L1}$ and ω_{zL2} only affects the range of allowed frequency; the region of allowed frequencies is shown by the bar with double arrows.

$531\ cm^{-1}$ $559\ cm^{-1}$ $734\ cm^{-1}$ $741\ cm^{-1}$
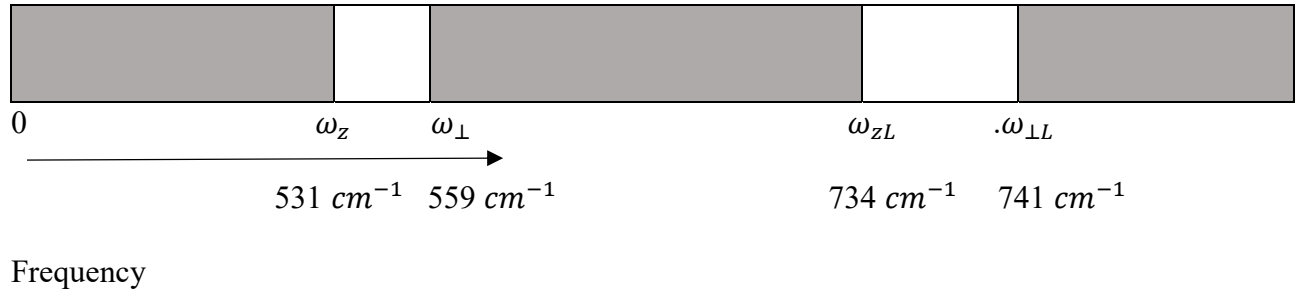
Frequency

Figure 22 Shaded region showing the range of frequencies for which $\varepsilon_\parallel \varepsilon_\perp > 0$ in GaN.

$$0 \qquad \omega_z \quad \omega_\perp \qquad\qquad\qquad \omega_{zL} \qquad \omega_{\perp L}$$

$$531\ cm^{-1}\ 559\ cm^{-1} \qquad\qquad 734\ cm^{-1} \quad 741\ cm^{-1}$$
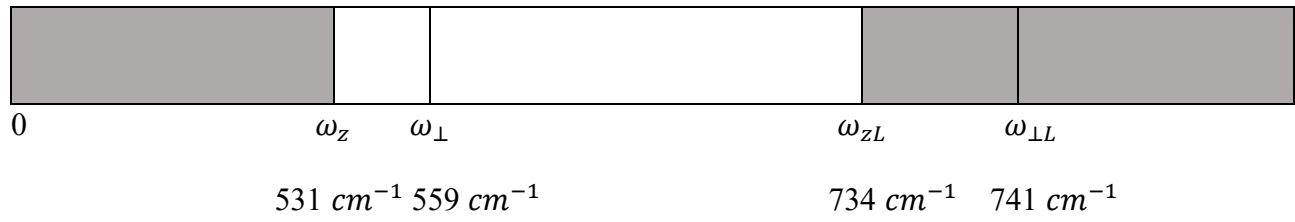
Figure 23 Shaded region showing the range of frequencies for which $\varepsilon_\parallel > 0$ in GaN

However, it is emphasized here that the above relations between $\epsilon_\parallel \epsilon_\perp > 0$ and ω as well as $\epsilon_\parallel > 0$ and ω hold for every wurtzite material.

$$\omega_\perp = 559\ cm^{-1} \qquad\qquad \omega_{zL} = 734\ cm^{-1}$$

$$\omega_z$$

$$\omega_\perp = 559\ cm^{-1} \qquad\qquad \omega_{zL} = 734\ cm^{-1}$$
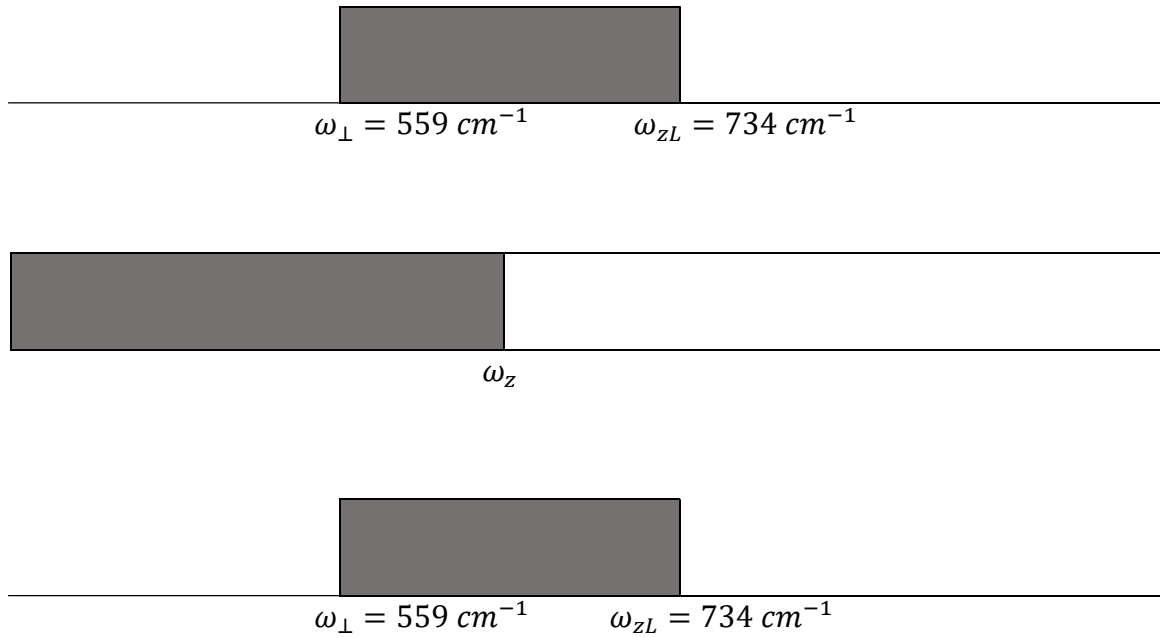
Figure 24 Arrangement of three layers for Type A: First Case.

$$\omega_\perp = 559 \; cm^{-1} \qquad \omega_{zL} = 734 \; cm^{-1}$$

$$\omega_{\perp L}$$

$$\omega_\perp = 559 \; cm^{-1} \qquad \omega_{zL} = 734 \; cm^{-1}$$

Range: $734 - \omega_{\perp L}(In_x Ga_{1-x}N)$
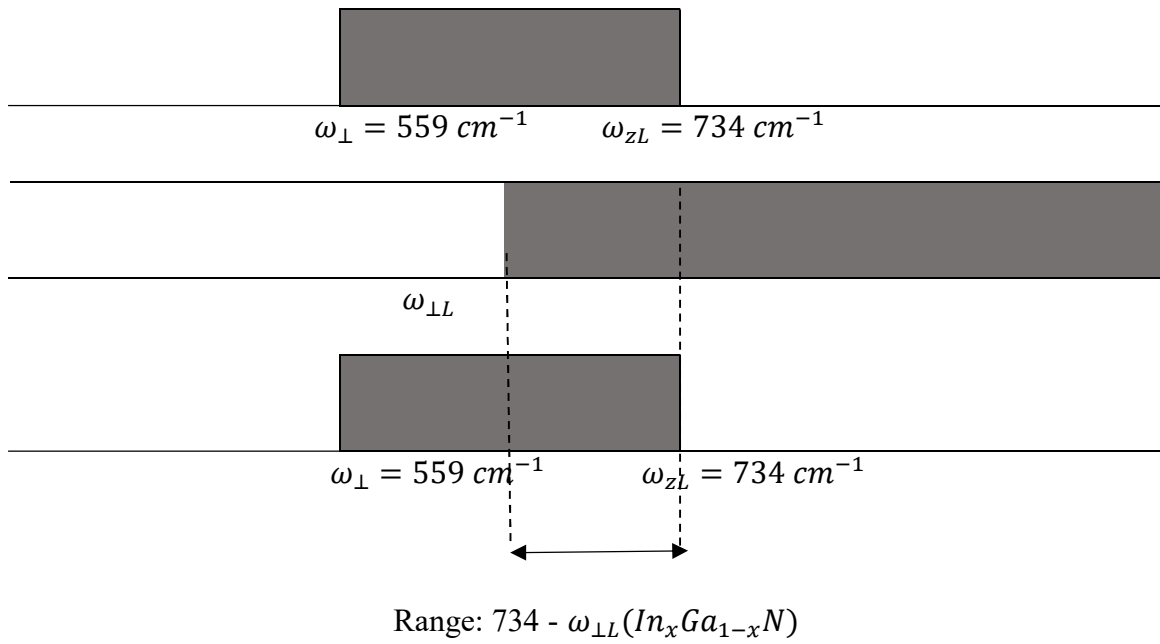
Figure 25 Arrangement of three layers for Type A: Second Case

The region of allowed frequencies is shown by the bar with double arrows.

$$\omega_z = 531 \; cm^{-1}$$

$$\omega_\perp \qquad\qquad \omega_{zL}$$

$$\omega_z = 531 \; cm^{-1}$$

Range $= 531 \; cm^{-1} - \omega_\perp$
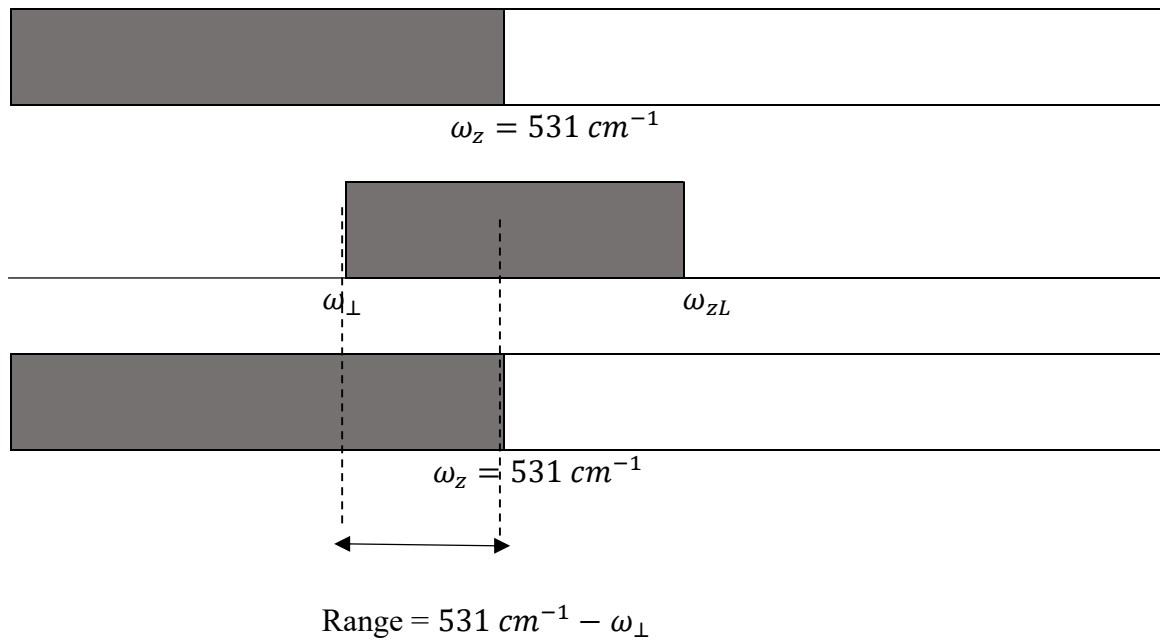
Figure 26 Arrangement of three layers for Type B: First Case

The region of allowed frequencies is shown by the bar with double arrows.

$\omega_{\perp L} = 741\ cm^{-1}$

$\omega_{\perp}$

ω_{zL}

$\omega_{\perp L} = 741\ cm^{-1}$

Range $= \omega_{zL} - 741\ cm^{-1}$
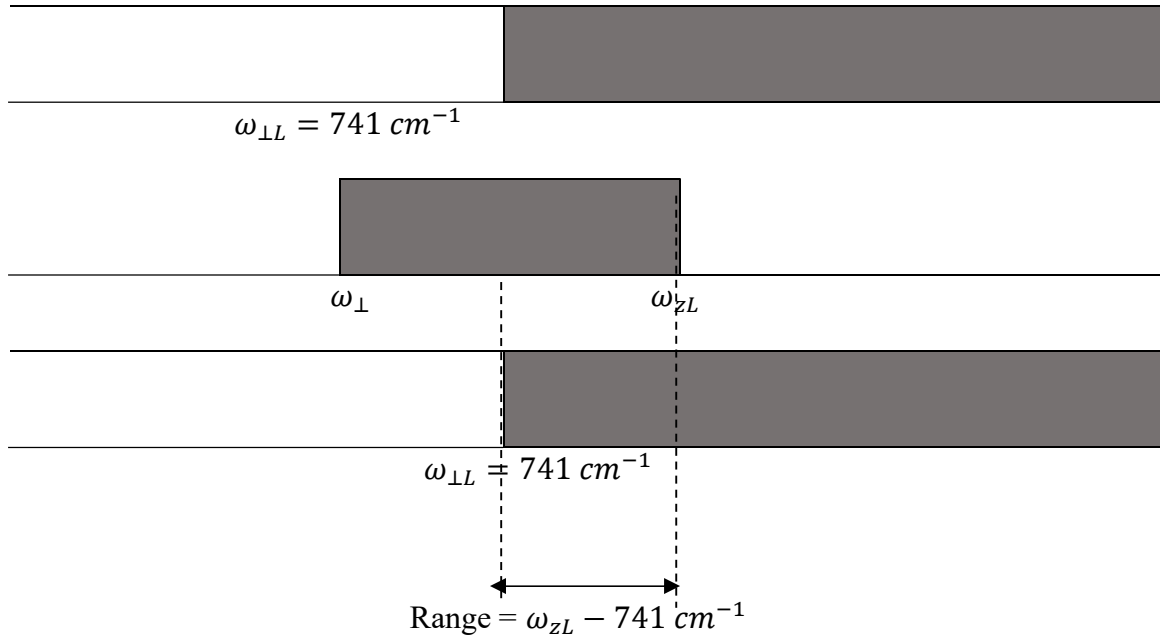
Figure 27 Arrangement of three layers for Type B: Second Case

The region of allowed frequencies is shown by the bar with double arrows.

CHAPTER 3 INTERFACE PHONONS IN METAL TERMINATED TWO INTERFACE WURTZITE HETEROSTRUCTURE

3.1 INTRODUCTION

In this chapter a metal-terminated two-interface wurtzite heterostructure as shown in Fig. 28 is considered and analytical expressions for dispersion relations for interface modes will be derived and after that Frohlich potential expressions will be derived. The mathematical analysis in this chapter is described in detail; however, the steps are same as that in Chapter 2.

3.2 ANALYSIS
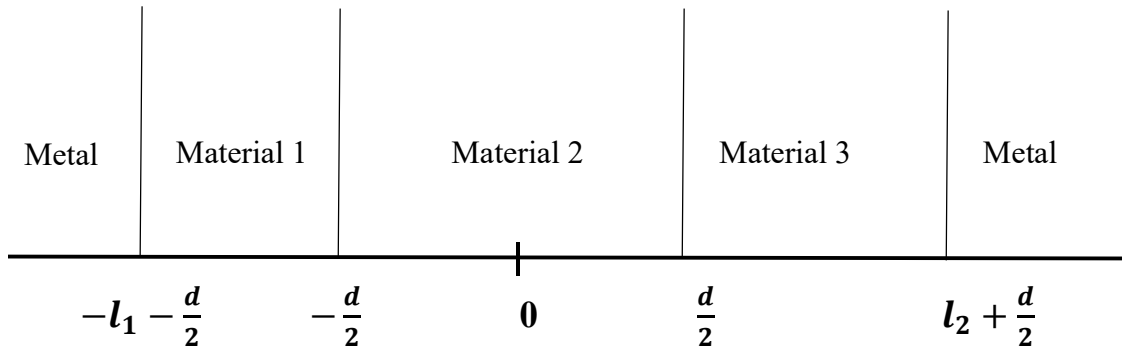
Figure 28 Metal-terminated two-interface heterostructure with reference coordinate axes.

In the notation of the macroscopic dielectric continuum model, the classical electrostatic equations which are satisfied by the polar optical phonon fields [1, 10-13] are,

$$\vec{E}(\vec{r}) = -\nabla\Phi(\vec{r}) \tag{20}$$

$$\vec{D}(\vec{r}) = \vec{E}(\vec{r}) + 4\pi P(\vec{r}) = \varepsilon_\perp(\omega)E_\perp(\vec{r})\hat{\rho} + \varepsilon_z(\omega)E_z(\vec{r})\hat{z} \tag{21}$$

$$\nabla.\vec{D}(\vec{r}) = 0 \tag{22}$$

where Φ is the potential introduced by the optical phonon modes, E represents electric field, D

represents displacement field and P represents polarization field. Where, $\hat{\rho}$ and $\hat{z}$ represent the

unit vectors perpendicular to and parallel to z- axis (which is also c-axis) respectively.

Substituting the equation for the electrostatic phonon potential $\Phi(r) = \Phi(z)e^{i\vec{q}\cdot\vec{\rho}}$

into Eq. 20, one finds

$$\nabla \cdot \vec{D} = \left(\varepsilon_z(\omega)\frac{\partial^2}{\partial z^2} - \varepsilon_\perp(\omega)q^2 \right)\Phi(\vec{r}) = 0 \tag{23}$$

Taking into account boundary conditions at $z = \pm\infty$, $\Phi(z)\big|_{z\to\pm\infty} = 0$

It follows that for wurzite heterstructures as depicted in Fig. 28, that the phonon potential is:

$$\Phi(\vec{r}) = e^{i\vec{q}\cdot\vec{\rho}}\begin{cases} C \cosh\left(k_1 \left(z + \dfrac{d}{2} \right) \right) + D \sinh\left(k_1 \left(z + \dfrac{d}{2} \right) \right) & z < -d/2 \\ A \cosh(k_2 z) + B \sinh(k_2 z) & -\dfrac{d}{2} \le z \le d/2 \\ E \cosh\left(k_3 \left(z - \dfrac{d}{2} \right) \right) + F \sinh\left(k_3 \left(z - \dfrac{d}{2} \right) \right) & z > d/2 \end{cases} \tag{24}$$

where A, B, C, D, E and F are potential amplitudes in the various material regions and the

wavevectors in the three regions are denoted by k_1, k_2 and k_3.

The intermediate layer has a thickness, d. It should be noted that the metal regions are assumed

to be perfect conductors; hence, the potential is zero in the volume enclosed by metal region and

metal surface.

Applying the boundary conditions:

$$\Phi_i(z) = \Phi_{i+1}(z) \qquad (25)$$

$$\varepsilon_i \frac{\partial \Phi_i}{\partial z} = \varepsilon_{i+1} \frac{\partial \Phi_{i+1}}{\partial z} \qquad (26)$$

which express the facts that the normal component of D_z and the tangential component of $E_\perp$ are continuous at the interfaces. In continuation of above, applying boundary conditions at the following interfaces:

$$z = -l_1 - \frac{d}{2}$$

Continuity electric field:

$$C \cosh(k_1 l_1) - D \sinh(k_1 l_1) = 0$$

$$\Rightarrow C = D \tanh(k_1 l_1) \qquad (27)$$

It is to be noted that the normal component of the displacement field D_z is not continuous at metal-dielectric interface, because of the polarization field $\vec{P}$ inside the dielectric we have a surface charge density $\sigma = \vec{P}.\hat{n}$ at the metal-dielectric boundary. $\hat{n}$ represents unit vector normal to the metal surface directed from metal to dielectric.

$$z = -\frac{d}{2}$$

continuity of electric field:

$$C = A\,cosh\left(k_2\frac{d}{2}\right) - B\,sinh\left(k_2\frac{d}{2}\right) \tag{28}$$

From the continuity of the normal component of displacement field:

$$\varepsilon_{1z}k_1 D = \varepsilon_{2z}k_2\left(-A\,sinh\left(k_2\frac{d}{2}\right) + B\,cosh\left(k_2\frac{d}{2}\right)\right) \tag{29}$$

Substituting for D from Eq. 27 in Eq. 29 and then equating Eq.28 and Eq. 29, we get:

$$\frac{\varepsilon_{2z}k_2}{\varepsilon_{1z}k_1}\left(-A\,sinh\left(k_2\frac{d}{2}\right) + B\,cosh\left(k_2\frac{d}{2}\right)\right)tanh(k_1 l_1) = A\,cosh\left(k_2\frac{d}{2}\right) - B\,sinh\left(k_2\frac{d}{2}\right)$$

$$B = A\frac{\left(\varepsilon_{1z}k_1 + \varepsilon_{2z}k_2 tanh\left(k_2\frac{d}{2}\right)tanh(k_1 l_1)\right)}{\left(\varepsilon_{2z}k_2 tanh(k_1 l_1) + \varepsilon_{1z}k_1 tanh\left(k_2\frac{d}{2}\right)\right)} \tag{30}$$

$$z = +\frac{d}{2}$$

applying continuity of electric field:

$$E = A\,cosh\left(k_2\frac{d}{2}\right) + B\,sinh\left(k_2\frac{d}{2}\right) \tag{31}$$

Applying continuity of normal component of displacement field:

$$\varepsilon_{2z}k_2\left(A\,sinh\left(k_2\frac{d}{2}\right) + B\,cosh\left(k_2\frac{d}{2}\right)\right) = \varepsilon_{3z}k_3F \tag{32}$$

$$z = l_2 + \frac{d}{2}$$

applying continuity of electric field parallel to interface:

$$E\,cosh(k_3l_2) + F\,sinh(k_3l_2) = 0$$

$$\Rightarrow E = -F\,tanh(k_3l_2) \tag{33}$$

Substituting for F from Eq. 33 in Eq. 32 and then equating Eq. 31 and Eq. 32, we get:

$$-\frac{\varepsilon_{2z}k_2}{\varepsilon_{3z}k_3}\left(A \sinh\left(k_2\frac{d}{2}\right) + B \cosh\left(k_2\frac{d}{2}\right)\right)\tanh(k_3 l_2)$$

$$= A \cosh\left(k_2\frac{d}{2}\right) + B \sinh\left(k_2\frac{d}{2}\right)$$

$$B = -A\frac{\left(\varepsilon_{2z}k_2 \tanh\left(k_2\frac{d}{2}\right)\tanh(k_3 l_2) + \varepsilon_{3z}k_3\right)}{\left(\varepsilon_{2z}k_2 \tanh(k_3 l_2) + \varepsilon_{3z}k_3 \tanh\left(k_2\frac{d}{2}\right)\right)} \qquad (34)$$

Equating Eq. 30 and Eq. 34, we get:

$$\frac{\left(\varepsilon_{1z}k_1 + \varepsilon_{2z}k_2 \tanh\left(k_2\frac{d}{2}\right)\tanh(k_1 l_1)\right)}{\left(\varepsilon_{2z}k_2 \tanh(k_1 l_1) + \varepsilon_{1z}k_1 \tanh\left(k_2\frac{d}{2}\right)\right)} = -\frac{\left(\varepsilon_{2z}k_2 \tanh\left(k_2\frac{d}{2}\right)\tanh(k_3 l_2) + \varepsilon_{3z}k_3\right)}{\left(\varepsilon_{2z}k_2 \tanh(k_3 l_2) + \varepsilon_{3z}k_3 \tanh\left(k_2\frac{d}{2}\right)\right)}$$

$$(35)$$

The above expression is the dispersion relation of a metal-terminated two-interface heterostructure.

Obviously, the above dispersion relation must reduce to the dispersion relation of two-interface heterostructure terminated with semi-infinite layers (as obtained in Eq. 10) in the limits as $l_1 \to \infty$ and $l_2 \to \infty$. Applying these limits:

$$\lim_{l_1 \to \infty}\frac{\left(\varepsilon_{1z}k_1 + \varepsilon_{2z}k_2 \tanh\left(k_2\frac{d}{2}\right)\tanh(k_1 l_1)\right)}{\left(\varepsilon_{2z}k_2 \tanh(k_1 l_1) + \varepsilon_{1z}k_1 \tanh\left(k_2\frac{d}{2}\right)\right)} = \lim_{l_2 \to \infty} -\frac{\left(\varepsilon_{2z}k_2 \tanh\left(k_2\frac{d}{2}\right)\tanh(k_3 l_2) + \varepsilon_{3z}k_3\right)}{\left(\varepsilon_{2z}k_2 \tan\ (k_3 l_2) + \varepsilon_{3z}k_3 \tanh\left(k_2\frac{d}{2}\right)\right)}$$

Since, we know that: $\lim_{x \to \infty} tanh(x) = 1$, the above equation reduces to:

$$\frac{\left(\varepsilon_{1z}k_1 + \varepsilon_{2z}k_2 tanh\left(k_2 \frac{d}{2}\right)\right)}{\left(\varepsilon_{2z}k_2 + \varepsilon_{1z}k_1 tanh\left(k_2 \frac{d}{2}\right)\right)} = -\frac{\left(\varepsilon_{2z}k_2 tanh\left(k_2 \frac{d}{2}\right) + \varepsilon_{3z}k_3\right)}{\left(\varepsilon_{2z}k_2 + \varepsilon_{3z}k_3 tanh\left(k_2 \frac{d}{2}\right)\right)}$$

The above equation is same as case without metal case (as in Eq. 10)

To simplify the expression for the Frohlich potential, the potential in the middle layer, as in Equation 24, can be broken down in symmetric and anti-symmetric components. The symmetric component corresponds to B = 0 whereas the anti-symmetric component corresponds to A =0.

3.2.1 Symmetric Modes

To obtain the expressions for the symmetric modes the boundary conditions are satisfied at every interface, as shown below:

$$z = -\frac{d}{2}$$

Continuity of electric field parallel to interface: $\Phi_+ = C = A \cosh\left(k_2 \frac{d}{2}\right)$

$$A = \frac{\Phi_+}{\cosh\left(k_2 \frac{d}{2}\right)} \tag{36}$$

Continuity of normal component of displacement field:

$$\varepsilon_{1z}k_1 D = -\varepsilon_{2z}k_2\, A\, sinh\left(k_2\frac{d}{2}\right)$$

$$D = -\frac{\varepsilon_{2z}k_2}{\varepsilon_{1z}k_1}\, \Phi_+\, tanh\left(k_2\frac{d}{2}\right)$$

(37)

$z = -l_1 - \frac{d}{2}$

Continuity of electric field parallel to interface:

$$\Phi_+ = C = D\, \tanh(k_1 l_1)$$

$$D = \Phi_+\, \coth(k_1 l_1)$$

(38)

$z = +\frac{d}{2}$

Continuity of electric field parallel to interface:

$$A\ cosh\left(k_2\frac{d}{2}\right) = E$$

Substituting for A from Eq. 36, we obtain:

$$E = C = \Phi_+ \tag{37}$$

Continuity of normal component of displacement field:

$$\varepsilon_{2z}k_2\ A\ sinh\left(k_2\frac{d}{2}\right) = \varepsilon_{3z}k_3 F$$

Substituting for A from Eq. 18, we find:

$$F = \Phi_+\frac{\varepsilon_{2z}k_2}{\varepsilon_{3z}k_3}tanh\left(k_2\frac{d}{2}\right) \tag{38}$$

$$z = l_2 + \frac{d}{2}$$

Continuity of electric field parallel to interface:

$$E\ cosh(k_3 l_2) + F\ sinh(k_3 l_2) = 0$$

$$(39)$$

$$F = -E \, coth(k_3 l_2) = -\Phi_+ \, coth(k_3 l_2)$$

Now, the equation for symmetric modes can be written as:

$\Phi(\vec{r})$

$$= e^{i\vec{q}\cdot\vec{\rho}} \begin{cases} \Phi_+ \cosh\left(k_1\left(z+\dfrac{d}{2}\right)\right) + \Phi_+ \coth(k_1 l_1) \, \sinh\left(k_1\left(z+\dfrac{d}{2}\right)\right) & z < -d/2 \\[3ex] \dfrac{\Phi_+}{\cosh\left(k_2\dfrac{d}{2}\right)} \cosh(k_2 z) & -\dfrac{d}{2} \le z \le d/2 \\[3ex] \Phi_+ \cosh\left(k_3\left(z-\dfrac{d}{2}\right)\right) - \Phi_+ \coth(k_3 l_2) \, \sinh\left(k_3\left(z-\dfrac{d}{2}\right)\right) & z > d/2 \end{cases}$$

The expression for Φ_+ can be obtained after substituting the above expression in the normalization equation, which is:

$$\frac{\hbar}{2\omega L^2} = \sum \frac{1}{4\pi} \frac{1}{2\omega} \int_{R_i} dz \left(q^2 \frac{\partial \varepsilon_{i,\perp}(\omega)}{\partial \omega} |\Phi_i(q,z)|^2 + \frac{\partial \varepsilon_{i,z}(\omega)}{\partial \omega} \left| \frac{\partial \Phi_i(q,z)}{\partial z} \right|^2 \right) \qquad (40)$$

To solve for Φ_+, we will evaluate the respective integrals in each region of the heterostructure as in Fig. 28 as shown below:

Region I:

$$\int_{-l_1-\frac{d}{2}}^{\frac{d}{2}} |\Phi_1(z)|^2 dz =$$

$$C^2 \int_{-l_1}^{0} cosh^2(k_1 x)\, dx + D^2 \int_{-l_1}^{0} sinh^2(k_1 x)\, dx + CD \int_{-l_1}^{0} sinh(2k_1 x)\, dx$$

$$= C^2 \int_{-l_1}^{0} \left(\frac{cosh(2k_1 x) + 1}{2} \right) dx + D^2 \int_{-l_1}^{0} \left(\frac{cosh(2k_1 x) - 1}{2} \right) dx + \frac{CD}{2k_1} cosh(2k_1 x)]_{-l_1}^{0}$$

$$= \frac{C^2}{2} \left(\frac{sinh(2k_1 l_1)}{2k_1} + l_1 \right) + \frac{D^2}{2} \left(\frac{sinh(2k_1 l_1)}{2k_1} - l_1 \right) - \frac{CD}{k_1} sinh^2(k_1 l_1) \qquad (41)$$

Substituting $\Phi_+ = C$ and $D = \Phi_+ coth(k_1 l_1)$ in the above equation, we obtain:

$$\int_{-l_1-\frac{d}{2}}^{\frac{d}{2}} |\Phi_1(z)|^2 dz =$$

$$\left(\frac{1}{2}\left(\frac{sinh(2k_1l_1)}{2k_1} + l_1\right) + \frac{coth^2(k_1l_1)}{2}\left(\frac{sinh(2k_1l_1)}{2k_1} - l_1\right) - \frac{coth(k_1l_1)}{k_1}\ sinh^2(k_1l_1)\right)\Phi_+^2$$

$$(42)$$

$$\int_{-l_1-\frac{d}{2}}^{\frac{d}{2}} \left|\frac{\partial\Phi_1(z)}{\partial z}\right|^2 dz =$$

$$k_1^2\left[C^2\int_{-l_1}^{0} sinh^2(k_1x)\ dx +\ D^2\int_{-l_1}^{0} cosh^2(k_1x)\ dx +\ CD\int_{-l_1}^{0} sinh(2k_1x)\ dx\right]$$

$$= k_1^2\left[\frac{C^2}{2}\left(\frac{sinh(2k_1l_1)}{2k_1} - l_1\right) + \frac{D^2}{2}\left(\frac{sinh(2k_1l_1)}{2k_1} + l_1\right) - \frac{CD}{k_1}sinh^2(k_1l_1)\right]$$

$$\Phi_+^2\ k_1^2\left[\frac{1}{2}\left(\frac{sinh(2k_1l_1)}{2k_1} - l_1\right) + \frac{coth^2(k_1l_1)}{2}\left(\frac{sinh(2k_1l_1)}{2k_1} + l_1\right)\right.$$

$$\left. - \frac{coth(k_1l_1)}{k_1}sinh^2(k_1l_1)\right]$$

$$(43)$$

Region II

$$\int_{-\frac{d}{2}}^{\frac{d}{2}}|\Phi_2(z)|^2 dz = A^2 \int_{-d/2}^{d/2} cosh^2(k_2 z)\, dz = A^2 \left(\frac{sinh(k_2 d)}{2} + \frac{d}{2} \right)$$

$$= \frac{\Phi_+{}^2}{cosh^2\left(k_2\frac{d}{2}\right)} \left(\frac{sinh(k_2 d)}{2} + \frac{d}{2} \right) \qquad (44)$$

$$\int_{-\frac{d}{2}}^{\frac{d}{2}}\left|\frac{\partial \Phi_2(z)}{\partial z}\right|^2 dz = A^2 k_2^2 \int_{-d/2}^{d/2} sinh^2(k_2 z)\, dz = A^2 k_2^2 \left(\frac{sinh(k_2 d)}{2} - \frac{d}{2} \right)$$

$$= \frac{\Phi_+{}^2 k_2^2}{cosh^2\left(k_2\frac{d}{2}\right)} \left(\frac{sinh(k_2 d)}{2} - \frac{d}{2} \right) \qquad (45)$$

Region III

$$\int_{+\frac{d}{2}}^{l_2+\frac{d}{2}}|\Phi_3(z)|^2 dz = E^2 \int_0^{l_2} cosh^2(k_3 x)dx + F^2 \int_0^{l_2} sinh^2(k_3 x)dx + EF \int_0^{l_2} sinh(k_3 x)\, dx$$

$$= \frac{E^2}{2}\left(\frac{sinh(2k_3 l_2)}{2k_3} + l_2\right) + \frac{F^2}{2}\left(\frac{sinh(2k_3 l_2)}{2k_3} - l_2\right) + \frac{EF}{k_3} sinh^2(k_3 l_2)$$

$$= \left(\frac{1}{2}\left(\frac{sinh(2k_3 l_2)}{2k_3} + l_2\right) + \frac{coth^2(k_3 l_2)}{2}\left(\frac{sinh(2k_3 l_2)}{2k_3} - l_2\right) - \frac{coth(k_3 l_2)}{k_3} sinh^2(k_3 l_2)\right)\Phi_+^2$$

$$(46)$$

$$\int_0^{l_2} \left|\frac{\partial \Phi_3(z)}{\partial z}\right|^2 = k_3^2 \left(E^2 \int_0^{l_2} sinh^2(k_3 x)\, dx + F^2 \int_0^{l_2} cosh^2(k_3 x)\, dx + EF \int_0^{l_2} sinh(2k_3 x)\, dx\right)$$

$$= k_3^2 \left(\frac{E^2}{2}\left(\frac{sinh(2k_3 l_2)}{2k_3} - l_2\right) + \frac{F^2}{2}\left(\frac{sinh(2k_3 l_2)}{2k_3} + l_2\right) + \frac{EF}{k_3} sinh^2(k_3 l_2)\right)$$

$$= \Phi_+^2 k_3^2 \left(\frac{1}{2}\left(\frac{sinh(2k_3 l_2)}{2} - l_2\right) + \frac{coth^2(k_3 l_2)}{2}\left(\frac{sinh(2k_3 l_2)}{2} + l_2\right)\right.$$

$$\left. - \frac{coth(k_3 l_2)}{k_3} sinh^2(k_1 l_2)\right)$$

$$(47)$$

From Equation 40:

$$\frac{\hbar}{2\omega L^2} = \sum \frac{1}{4\pi} \frac{1}{2\omega} \int_{R_i} dz \left(q^2 \frac{\partial \varepsilon_{i,\perp}(\omega)}{\partial \omega} |\Phi_i(q,z)|^2 + \frac{\partial \varepsilon_{i,z}(\omega)}{\partial \omega} \left|\frac{\partial \Phi_i(q,z)}{\partial z}\right|^2\right)$$

$$\Phi_+ L = \sqrt{\frac{2h}{\varepsilon_0}\left[\left(q^2\frac{\partial\varepsilon_{1,\perp}}{\partial\omega}I_1 + \frac{\partial\varepsilon_{1,z}}{\partial\omega}I_1'\right) + \left(q^2\frac{\partial\varepsilon_{2,\perp}}{\partial\omega}I_2 + \frac{\partial\varepsilon_{2,z}}{\partial\omega}I_2'\right)\right.}$$

$$\left. + \left(q^2\frac{\partial\varepsilon_{3,\perp}}{\partial\omega}I_3 + \frac{\partial\varepsilon_{3,z}}{\partial\omega}I_3'\right)\right]^{-\frac{1}{2}}$$

where:

$$I_1 = \frac{1}{2}\left(\frac{sinh(2k_1l_1)}{2k_1} + l_1\right) + \frac{coth^2(k_1l_1)}{2}\left(\frac{sinh(2k_1l_1)}{2k_1} - l_1\right) - \frac{coth(k_1l_1)}{k_1}sinh^2(k_1l_1)$$

$$I_1' = k_1^2\left[\frac{1}{2}\left(\frac{sinh(2k_1l_1)}{2k_1} - l_1\right) + \frac{coth^2(k_1l_1)}{2}\left(\frac{sinh(2k_1l_1)}{2k_1} + l_1\right) - \frac{coth(k_1l_1)}{k_1}sinh^2(k_1l_1)\right]$$

$$I_2 = \frac{1}{cosh^2\left(k_2\frac{d}{2}\right)}\left(\frac{sinh(k_2d)}{2k_2} + \frac{d}{2}\right)$$

$$I_2' = \frac{k_2^2}{cosh^2\left(k_2\frac{d}{2}\right)}\left(\frac{sinh(k_2d)}{2k_2} - \frac{d}{2}\right)$$

$$I_3 = \frac{1}{2}\left(\frac{sinh(2k_3l_2)}{2k_3} + l_2\right) + \frac{coth^2(k_3l_2)}{2}\left(\frac{sinh(2k_3l_2)}{2k_3} - l_2\right) - \frac{coth(k_3l_2)}{k_3}sinh^2(k_3l_2)$$

$$I_3' = k_3^2 \left(\frac{1}{2} \left(\frac{sinh(2k_3l_2)}{2k_3} - l_2 \right) + \frac{coth^2(k_3l_2)}{2} \left(\frac{sinh(2k_3l_2)}{2k_3} + l_2 \right) - \frac{coth(k_3l_2)}{k_3} sinh^2(k_3l_2) \right)$$

3.2.2 Anti-symmetric modes:

The anti-symmetric modes corresponds to A=0 in Equation 24 . After setting A = 0 for potential in the middle layer and applying electrostatic boundary conditions as in the previous paragraph we obtain the following relations:

$$C = -\Phi_-$$

(49)

$$D = -\Phi_- coth(k_1l_1)$$

(50)

$$B = \frac{\Phi_-}{sinh \left(k_2 \frac{d}{2} \right)}$$

(51)

$$E = \Phi_-$$

(52)

$$F = -\Phi_- coth(k_3l_2)$$

(53)

Thus, the phonon potential for anti-symmetric mode can be expressed as:

$$\Phi(\vec{r})$$

$$= e^{i\vec{q}\cdot\vec{\rho}} \begin{cases} -\Phi_- \cosh\left(k_1\left(z+\frac{d}{2}\right)\right) - \Phi_- \coth(k_1 l_1) \, \sinh\left(k_1\left(z+\frac{d}{2}\right)\right) & z < -d/2 \\[2em] \dfrac{\Phi_-}{\sinh\left(k_2\frac{d}{2}\right)} \sinh(k_2 z) & -\dfrac{d}{2} \leq z \leq d/2 \\[2em] \Phi_- \cosh\left(k_3\left(z-\frac{d}{2}\right)\right) - \Phi_- \coth(k_3 l_2) \sinh\left(k_3\left(z-\frac{d}{2}\right)\right) & z > d/2 \end{cases}$$

When subjected to the normalization condition, we obtain:

$$\Phi_- L = \sqrt{\frac{2h}{\varepsilon_0}} \left[\left(q^2 \frac{\partial\varepsilon_{1,\perp}}{\partial\omega} I_1 + \frac{\partial\varepsilon_{1,z}}{\partial\omega} I'_1 \right) + \left(q^2 \frac{\partial\varepsilon_{2,\perp}}{\partial\omega} I_2 + \frac{\partial\varepsilon_{2,z}}{\partial\omega} I'_2 \right) \right.$$

$$\left. + \left(q^2 \frac{\partial\varepsilon_{3,\perp}}{\partial\omega} I_3 + \frac{\partial\varepsilon_{3,z}}{\partial\omega} I'_3 \right) \right]^{-\frac{1}{2}} \tag{54}$$

where:

$$I_1 = \frac{1}{2}\left(\frac{sinh(2k_1 l_1)}{2k_1} + l_1\right) + \frac{coth^2(k_1 l_1)}{2}\left(\frac{sinh(2k_1 l_1)}{2k_1} - l_1\right) - \frac{coth(k_1 l_1)}{k_1} \, sinh^2(k_1 l_1)$$

$$I'_1 = k_1^2\left[\frac{1}{2}\left(\frac{sinh(2k_1 l_1)}{2k_1} - l_1\right) + \frac{coth^2(k_1 l_1)}{2}\left(\frac{sinh(2k_1 l_1)}{2k_1} + l_1\right) - \frac{coth(k_1 l_1)}{k_1} sinh^2(k_1 l_1)\right]$$

$$I_2 = \frac{1}{sinh^2\left(k_2\frac{d}{2}\right)}\left(\frac{sinh(k_2d)}{2k_2} - \frac{d}{2}\right)$$

$$I_2' = \frac{k_2^2}{sinh^2\left(k_2\frac{d}{2}\right)}\left(\frac{sinh(k_2d)}{2k_2} + \frac{d}{2}\right)$$

$$I_3 = \frac{1}{2}\left(\frac{sinh(2k_3l_2)}{2k_3} + l_2\right) + \frac{coth^2(k_3l_2)}{2}\left(\frac{sinh(2k_3l_2)}{2k_3} - l_2\right) - \frac{coth(k_3l_2)}{k_3}sinh^2(k_3l_2)$$

$$I_3' = k_3^2\left(\frac{1}{2}\left(\frac{sinh(2k_3l_2)}{2k_3} - l_2\right) + \frac{coth^2(k_3l_2)}{2}\left(\frac{sinh(2k_3l_2)}{2k_3} + l_2\right) - \frac{coth(k_3l_2)}{k_3}sinh^2(k_3l_2)\right)$$

3.3 Dispersion relation for symmetric and anti-symmetric mode:

The dispersion relation for the symmetric and anti-symmetric modes can be derived directly from the secular equation and the same can be verified from the Frohlich potential equations of the respective modes. The derivation of the dispersion relation for each mode is shown below:

- **Symmetric mode:** As stated in the preceding paragraph, the condition for symmetric mode is obtained by setting B =0 in Frohlich potential equation of the middle layer. From Equation (12) and (16) it is observed that:

$$\left(\varepsilon_{1z} k_1 + \varepsilon_{2z} k_2 \tanh\left(k_2 \frac{d}{2}\right) \tanh(k_1 l_1) \right) \left(\varepsilon_{2z} k_2 \, \tanh\left(k_2 \frac{d}{2}\right) \tanh(k_3 l_2) + \varepsilon_{3z} k_3 \right) = 0$$

$$(55)$$

The above result is also obtained from the Frohlich potential equations for the symmetric mode, as follows:

Eliminating D from Eq. 37 and Eq. 38:

$$-\varepsilon_{2z} k_2 \tanh\left(k_2 \frac{d}{2}\right) = \varepsilon_1 k_1 \coth(k_1 l_1)$$

$$\Rightarrow \quad \varepsilon_{1z} k_1 + \varepsilon_{2z} k_2 \tanh\left(k_2 \frac{d}{2}\right) \tanh(k_1 l_1) = 0$$

Eliminating F from Eq. 38 and Eq. 39:

$$\varepsilon_{2z} k_2 \tanh\left(k_2 \frac{d}{2}\right) = -\varepsilon_{3z} k_3 \coth(k_3 l_2)$$

$$\Rightarrow \quad \varepsilon_{3z} k_3 + \varepsilon_{2z} k_2 \tanh\left(k_2 \frac{d}{2}\right) \tanh(k_3 l_2) = 0$$

We see that the above two equations must simultaneously vanish (equate to zero) for existence of symmetric modes thus their product must also vanish simultaneously, thus:

$$\Rightarrow \quad \left(\varepsilon_{1z} k_1 + \varepsilon_{2z} k_2 \tanh\left(k_2 \frac{d}{2}\right) \tanh(k_1 l_1) \right) \left(\varepsilon_{3z} k_3 + \varepsilon_{2z} k_2 \tanh\left(k_2 \frac{d}{2}\right) \tanh(k_3 l_2) \right) = 0$$

- **Anti-symmetric mode:** As stated in preceding paragraph, the condition for anti-symmetric mode is obtained by setting A =0 in Frohlich potential equation of the middle layer. From equation (30) and (34) it is observed that:

$$\left(\varepsilon_{2z}k_2\tanh(k_1l_1) + \varepsilon_{1z}k_1\tanh\left(k_2\frac{d}{2}\right)\right)\left(\varepsilon_{2z}k_2\tanh(k_3l_2) + \varepsilon_{3z}k_3\tanh\left(k_2\frac{d}{2}\right)\right) = 0$$

The above result is also obtained from the Frohlich potential equations of the anti-symmetric mode. However, the derivation steps of anti-symmetric modes are similar to those of the symmetric modes; hence, those steps have not been shown. Similar to the case of the symmetric mode, the anti-symmetric mode case results in two simultaneous equations:

$$\left(\varepsilon_{2z}k_2\tanh(k_1l_1) + \varepsilon_{1z}k_1\tanh\left(k_2\frac{d}{2}\right)\right) = 0 \text{ and } \left(\varepsilon_{2z}k_2\tanh(k_3l_2) + \varepsilon_{3z}k_3\tanh\left(k_2\frac{d}{2}\right)\right) = 0$$

From which can be argued (under simultaneous agreement) that:

$$\left(\varepsilon_{2z}k_2\tanh(k_1l_1) + \varepsilon_{1z}k_1\tanh\left(k_2\frac{d}{2}\right)\right)\left(\varepsilon_{2z}k_2\tanh(k_3l_2) + \varepsilon_{3z}k_3\tanh\left(k_2\frac{d}{2}\right)\right) = 0$$

3.4 Application

The above equations for dispersion relations and the associated Frohlich potentials are hereby applied to a heterostructure with following parameters:

Layer 1 = $In_{0.15}Ga_{0.85}N$

Layer 2 = GaN

Layer3 = $In_{0.15}Ga_{0.85}N$

L1 = 10 nm

L2 =12 nm

The dispersion relation and the plot of symmetric and anti-symmetric modes for qd = 0.7 are plotted in the figure below:
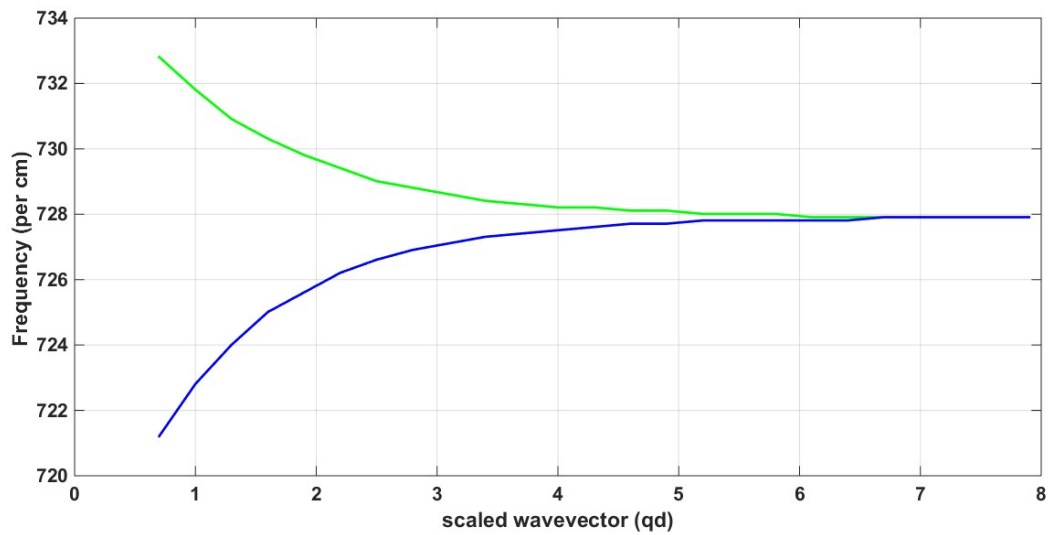
Figure 29 Dispersion relation for Metal/In0.15Ga0.5N/GaN/ In0.15Ga0.5N/Metal structure.

The blue line corresponds to the anti-symmetric mode and the green line corresponds to the symmetric mode
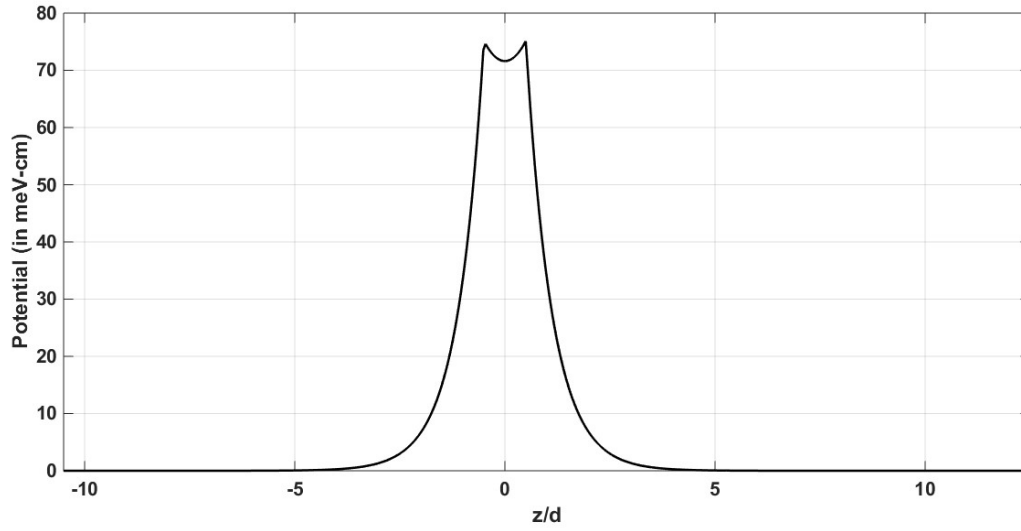
Figure 30 Symmetric potential in Metal/In0.15Ga0.5N/GaN/ In0.15Ga0.5N/Metal structure for qd=0.7
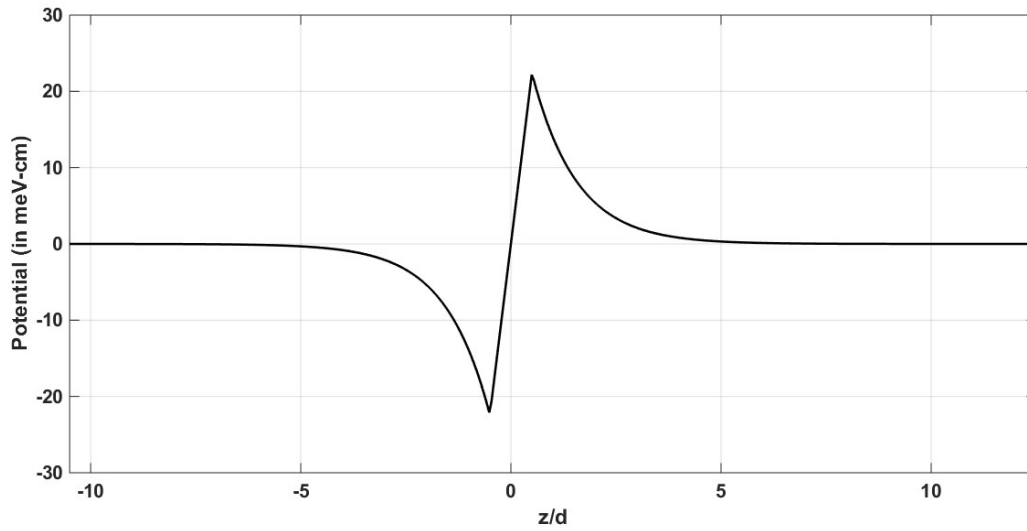
Figure 31 Anti-symmetric potential in Metal/In0.15Ga0.5N/GaN/ In0.15Ga0.5N/Metal structure for qd=0.7

3.5 Conditions for existence of interface phonons

It is observed from the expressions for the amplitudes of the symmetric and the anti-Symmetric potential that the interface phonon can exist in the metal terminated GaN/In0.15Ga0.85N/GaN only for those pairs of ω and q - as obtained from the dispersion relation - for which the amplitude of the Frohlich potential is a real number. Imposing this condition (amplitude must be real number) we get the following inequality:

$$\frac{\lambda_1}{2}\left(\frac{sinh(2k_1l_1)}{k_1} + \frac{sinh(2k_3l_2)}{k_3}\right)$$

$$\leq \frac{\lambda_{k1}}{2}\left(\frac{sinh(2k_1l_1)}{k_1} + \frac{coth^2(k_1l_1)}{2k_1}sinh(2k_1l_1)\right) - \frac{l_1}{4}\mu_{k1}cosech^2(k_1l_1)$$

$$+ \frac{\lambda_{k3}}{2}\left(\frac{sinh(2k_3l_2)}{k_3} + \frac{coth^2(k_3l_2)}{2k_3}sinh(2k_3l_2)\right) - \frac{l_2}{4}\mu_{k1}cosech^2(k_3l_2)$$

where,

$$\lambda_i = q^2\frac{\partial\varepsilon_{\perp,i}}{\partial\omega} + \frac{\partial\varepsilon_{z,i}}{\partial\omega}$$

$$\lambda_{ki} = q^2\frac{\partial\varepsilon_{\perp,i}}{\partial\omega} + k_i^2\frac{\partial\varepsilon_{z,i}}{\partial\omega}$$

$$\mu_{ki} = q^2\frac{\partial\varepsilon_{\perp,i}}{\partial\omega} - k_i^2\frac{\partial\varepsilon_{z,i}}{\partial\omega}$$

If the above inequality is violated, then the interface modes cease to exist in this heterostructure. However, it is observed from the dispersion relation that since the phonon frequencies for the

anti-symmetric mode is always less than the corresponding symmetric mode, the above inequality is never violated by anti-symmetric mode for any combination of l_1 and l_2.

CHAPTER 4 Transfer Matrix Theory for Wurtzite Multi-Interface Heterostructures

4.1 Introduction

In this chapter a general theory is developed which can be applied to any wurtzite heterostructure of any arbitrary number of 'n' layers to obtain the secular equation. Further, the equations will be applied to a 4-period AlN/GaN superlattice.

4.2 Analysis

Consider a superlattice consisting of n layers and let the reference co-ordinate axis be fixed to the first interface of the superlattice. Let the z-axis coincide with the c-axis of the wurtzite materials in the superlattice.

Figure 32 n-layer superlattice of wurtzite material with reference coordinate axes
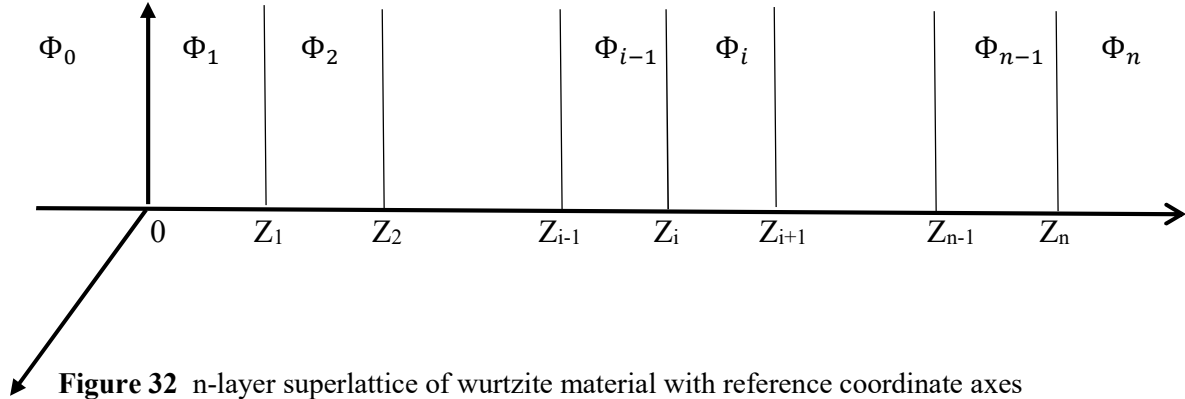
Let R_i represents the region enclosed by $z = z_{i+1}$ and z_i.

Let the thickness of the ith layer is $d_i = z_{i+1} - z_i$

Let Φ_i represents the phonon potential in the ith layer.

We know that, the phonon potential has the form: $\Phi(r) = \Phi(z)e^{i\vec{q}\cdot\vec{\rho}}$ for any region confined in z

direction, thus we can write the phonon potential for the ith layer as: $\Phi_i(r) = \Phi_i(z)e^{i\vec{q}\cdot\vec{\rho}}$.

4.2.1 Observation:

■ To find $\Phi_i(z)$, we need to solve Poisson's equation $\nabla^2\Phi_i = 0$ in the region R_i.

■ We must consider the fact that mathematically R_i is defined as:

$$R_i \in \{x, y, z_{i-1} \leq z \leq z_i\}$$

⇨ For region $R_{i:}$ $\nabla \equiv \dfrac{\partial}{\partial\rho}\,\hat{\boldsymbol{\rho}} + \dfrac{\partial}{\partial z'}\,\hat{\boldsymbol{z'}}$, where $z' = z - z_i$

When $\Phi_i(r)$ is substituted in the, we have:

$$\left(\varepsilon_{z,i}(\omega)\frac{\partial^2}{\partial z'^2} - \varepsilon_{\perp,i}(\omega)q^2\right)\Phi_i(z) = 0$$

⇨ $\left(\dfrac{\partial^2}{\partial z'^2} - k_i^2\right)\Phi_i(z') = 0$, where $k_i^2 = \dfrac{\varepsilon_{\perp,i}}{\varepsilon_{z,i}}q^2$

⇨ $\Phi_i(z') = A_i \exp(k_i z') + B_i \exp(-k_i z')$

⇨ $\boldsymbol{\Phi_i(z) = A_i \exp\big(k_i(z - z_i)\big) + B_i \exp\big(-k_i(z - z_i)\big)}$ (55)

Applying electrostatic boundary conditions at $z = z_{i+1}$:

(a) **Continuity of electric field parallel to interface:**

$$\Phi_i(z_{i+1}) = \Phi_{i+1}(z_{i+1})$$

$$A_i \exp\big(k_i(z_{i+1} - z_i)\big) + B_i \exp\big(-k_i(z_{i+1} - z_i)\big) = A_{i+1} + B_{i+1}$$

$$A_i \exp(k_i d_i) + B_i \exp(-k_i d_i) = A_{i+1} + B_{i+1}$$

(b) **Continuity of normal component of displacement field:**

$$\varepsilon_i k_i \, A_i \exp(k_i d_i) - \varepsilon_i k_i B_i \exp(-k_i d_i) = \varepsilon_{i+1} k_{i+1} A_{i+1} - \varepsilon_{i+1} k_{i+1} \, B_{i+1}$$

The above two equations can be expressed in matrix form as below:

$$\begin{bmatrix} \exp(k_i d_i) & \exp(-k_i d_i) \\ \varepsilon_i k_i \exp(k_i d_i) & -\varepsilon_i k_i \exp(k_i d_i) \end{bmatrix} \begin{bmatrix} A_i \\ B_i \end{bmatrix} = \begin{bmatrix} 1 & 1 \\ \varepsilon_{i+1} k_{i+1} & -\varepsilon_{i+1} k_{i+1} \end{bmatrix} \begin{bmatrix} A_{i+1} \\ B_{i+1} \end{bmatrix}$$

$$\begin{bmatrix} A_{i+1} \\ B_{i+1} \end{bmatrix} = \begin{bmatrix} 1 & 1 \\ \varepsilon_{i+1} k_{i+1} & -\varepsilon_{i+1} k_{i+1} \end{bmatrix}^{-1} \begin{bmatrix} \exp(k_i d_i) & \exp(-k_i d_i) \\ \varepsilon_i k_i \exp(k_i d_i) & -\varepsilon_i k_i \exp(k_i d_i) \end{bmatrix} \begin{bmatrix} A_i \\ B_i \end{bmatrix}$$

$$\begin{bmatrix} A_{i+1} \\ B_{i+1} \end{bmatrix} = \frac{1}{2\varepsilon_{i+1}k_{i+1}} \begin{bmatrix} \varepsilon_{i+1}k_{i+1} & 1 \\ \varepsilon_{i+1}k_{i+1} & -1 \end{bmatrix} \begin{bmatrix} \exp(k_i d_i) & \exp(-k_i d_i) \\ \varepsilon_i k_i \exp(k_i d_i) & -\varepsilon_i k_i \exp(k_i d_i) \end{bmatrix} \begin{bmatrix} A_i \\ B_i \end{bmatrix}$$

$$\begin{bmatrix} A_{i+1} \\ B_{i+1} \end{bmatrix} = \frac{1}{2\varepsilon_{i+1}k_{i+1}} \begin{bmatrix} (\varepsilon_{i+1}k_{i+1} + \varepsilon_i k_i)\exp(k_i d_i) & (\varepsilon_{i+1}k_{i+1} - \varepsilon_i k_i)\exp(-k_i d_i) \\ (\varepsilon_{i+1}k_{i+1} - \varepsilon_i k_i)\exp(k_i d_i) & (\varepsilon_{i+1}k_{i+1} + \varepsilon_i k_i)\exp(-k_i d_i) \end{bmatrix} \begin{bmatrix} A_i \\ B_i \end{bmatrix}$$

$$(56)$$

4.2.2 Derivation of secular equation:

Let,

$$[Q_i] = \frac{1}{2\varepsilon_{i+1}k_{i+1}} \begin{bmatrix} (\varepsilon_{i+1}k_{i+1} + \varepsilon_i k_i)\exp(k_i d_i) & (\varepsilon_{i+1}k_{i+1} - \varepsilon_i k_i)\exp(-k_i d_i) \\ (\varepsilon_{i+1}k_{i+1} - \varepsilon_i k_i)\exp(k_i d_i) & (\varepsilon_{i+1}k_{i+1} + \varepsilon_i k_i)\exp(-k_i d_i) \end{bmatrix}$$

$$[C_i] = \begin{bmatrix} A_i \\ B_i \end{bmatrix}$$

Thus,

$$[C_{i+1}] = [Q_i][C_i]$$

$$\Rightarrow [C_n] = [Q_{n-1}][Q_{n-2}][Q_{n-3}] \dots [Q_1][Q_0][C_0] \qquad (57)$$

where, $[C_0]$ and $[C_n]$ represents the Frohlich potential coefficient matrices of the end bulk regions on the extreme left and extreme right regions, respectively.

Since, $\Phi_0(z) = A_0 \exp(k_i z) + B_0 \exp(-k_i z)$ where z < 0, to ensure a finite potential of the phonon mode the above expression must converge to a finite limit when z $\rightarrow -\infty$ which leads to $B_0 = 0$. Similarly, $A_n = 0$.

We can write: $[Q_{n-1}][Q_{n-2}][Q_{n-3}] \ldots [Q_1][Q_0] = \begin{bmatrix} Q_{11} & Q_{12} \\ Q_{21} & Q_{22} \end{bmatrix}$

Thus,

$$\begin{bmatrix} 0 \\ B_n \end{bmatrix} = \begin{bmatrix} Q_{11} & Q_{12} \\ Q_{21} & Q_{22} \end{bmatrix} \begin{bmatrix} A_0 \\ 0 \end{bmatrix}$$

$\Rightarrow B_n = Q_{21} A_0$ and $Q_{11} A_0 = 0.$ \hfill (58)

For non-trivial solution of equation $Q_{11} A_0 = 0$, $|Q_{11}| = 0$.

Thus, the dispersion relation is given by:

$$|\boldsymbol{Q_{11}}| = \boldsymbol{0} \hspace{2cm} (59)$$

After obtaining the dispersion relation we can further extend our calculation to find the Frohlich amplitude. The following steps illustrates the method:

The interface modes must obey the normalization condition given below:

$$\frac{\hbar}{2\omega L^2} = \sum \frac{1}{4\pi} \frac{1}{2\omega} \int_{R_i} dz \left(q^2 \frac{\partial \varepsilon_{i,\perp}(\omega)}{\partial \omega} |\Phi_i(q,z)|^2 + \frac{\partial \varepsilon_{i,z}(\omega)}{\partial \omega} \left| \frac{\partial \Phi_i(q,z)}{\partial z} \right|^2 \right)$$

We proceed by evaluating the above integral for the ith layer bounded between $z = z_{i+1}$ & z_i

$$\int_{z_i}^{z_{i+1}} |\Phi_i|^2 dz = \int_{z_i}^{z_{i+1}} \left(A_i \exp(k_i(z - z_i)) + B_i \exp(-k_i(z - z_i)) \right)^2 dz$$

$$\int_{z_i}^{z_{i+1}} |\Phi_i|^2 dz = \frac{\sinh(k_i d_i)}{k_i} \left(A_i^2 \exp(k_i d_i) + B_i^2 \exp(-k_i d_i) \right) + 2A_i B_i d_i$$

Similarly,

$$\int_{z_i}^{z_{i+1}} \left| \frac{\partial \Phi_i(z)}{\partial z} \right|^2 dz = k_i^2 \int_{z_i}^{z_{i+1}} \left(A_i \exp(k_i(z - z_i)) - B_i \exp(-k_i(z - z_i)) \right)^2 dz \quad (60)$$

$$\int_{z_i}^{z_{i+1}} \left| \frac{\partial \Phi_i(z)}{\partial z} \right|^2 dz = k_i \sinh(k_i d_i) \left(A_i^2 \exp(k_i d_i) + B_i^2 \exp(-k_i d_i) \right) - 2A_i B_i d_i \quad (61)$$

From Eq. 57 we know that:

$$[C_i] = [Q_{i-1}][Q_{i-2}][Q_{i-3}] \dots [Q_1][Q_0][C_0]$$

Let, $[Q_{i-1}][Q_{i-2}][Q_{i-3}] \dots [Q_1][Q_0] = [Q_i]_T = \begin{bmatrix} Q_{i,11} & Q_{i,12} \\ Q_{i,21} & Q_{i,22} \end{bmatrix}$

Thus,

$$[C_i] = \begin{bmatrix} A_i \\ B_i \end{bmatrix} = [Q_i]_T [C_0] = \begin{bmatrix} Q_{i,11} & Q_{i,12} \\ Q_{i,21} & Q_{i,22} \end{bmatrix} \begin{bmatrix} A_0 \\ 0 \end{bmatrix}$$

Thus,

$$A_i = Q_{i,11} A_0 \text{ and } B_i = Q_{i,21} A_0$$

Substituting the above values of A_i and B_i in eq 60 and eq 61, obtain:

$$\int_{z_i}^{z_{i+1}} |\Phi_i|^2 dz = A_0^2 \left(\frac{sinh(k_i d_i)}{k_i} \left(Q_{i,11}^2 \, exp(k_i d_i) + Q_{i,21}^2 \, exp(-k_i d_i) \right) + 2Q_{i,11}Q_{i,21}d_i \right)$$

$$\int_{z_i}^{z_{i+1}} \left| \frac{\partial \Phi_i(z)}{\partial z} \right|^2 dz = A_0^2 \left(k_i sinh(k_i d_i) \left(Q_{i,11}^2 \, exp(k_i d_i) + Q_{i,21}^2 \, exp(-k_i d_i) \right) - 2Q_{i,11}Q_{i,21}d_i \right)$$

On substituting the above expression in the normalization equation we obtain the expression for

A_0:

$$A_0 = \sqrt{\frac{2h}{\varepsilon_0}} \left(\sum \int_{R_i} dz \left(q^2 \frac{\partial \varepsilon_{i,\perp}(\omega)}{\partial \omega} |\Phi_i(q,z)|^2 + \frac{\partial \varepsilon_{i,z}(\omega)}{\partial \omega} \left| \frac{\partial \Phi_i(q,z)}{\partial z} \right|^2 \right) \right)^{-1/2}$$

$$A_0 = \sqrt{\frac{2h}{\varepsilon_0}} \sum_{i=1}^{n} \left(q^2 \frac{\partial \varepsilon_{i,\perp}(\omega)}{\partial \omega} \left(\frac{sinh(k_i d_i)}{k_i} (Q_{i,11}^2 e^{k_i d_i} + Q_{i,21}^2 e^{-k_i d_i}) + 2Q_{i,11}Q_{i,21}d_i \right) \right.$$

$$\left. + \frac{\partial \varepsilon_{i,z}(\omega)}{\partial \omega} (k_i sinh(k_i d_i)(Q_{i,11}^2 e^{k_i d_i} + Q_{i,21}^2 e^{-k_i d_i}) - 2Q_{i,11}Q_{i,21}d_i) \right)^{-1/2}$$

$$(62)$$

If we perform the above summation over the number of layers, we can find the amplitude of the Frohlich potential of the interface mode, since the constants A_i and B_i can be expressed in terms of A_0.

4.3 Application of above equations on a superlattice:

The result so obtained above is applied to a heterostructure consisting of 4-periods of a 2-layer superlattice of AlN/GaN which is sandwiched between Air and $Al_{0.5}Ga_{0.5}N$:

Air	AlN	GaN	AlN	GaN	AlN	GaN	AlN	GaN	$Al_{0.5}Ga_{0.5}N$

Figure 33 A 4-period superlattice consisting of repeating layers of AlN/GaN

The thickness of the individual layers in the above heterostructure is 3-monolayers (0.75 nm)

$$[C_9] = [Q_8][Q_7] \, [Q_6][Q_5][Q_4][Q_3][Q_2][Q_1][Q_0][C_0]$$

In the above case:

$$[Q_1] = [Q_3] = [Q_5] = [Q_7] = \frac{1}{\alpha - \beta}\begin{bmatrix} \alpha \, exp(k_A d) & -\beta \, exp(-k_A d) \\ -\beta \, exp(k_A d) & \alpha \, exp(-k_A d) \end{bmatrix}$$

$$[Q_2] = [Q_4] = [Q_6] = \frac{1}{\alpha + \beta}\begin{bmatrix} \alpha \exp(k_B d) & -\beta \exp(-k_B d) \\ -\beta \exp(k_B d) & \alpha \exp(-k_B d) \end{bmatrix}$$

where, $\alpha = \varepsilon_A k_A + \varepsilon_B k_B$; $\beta = \varepsilon_A k_A - \varepsilon_B k_B$; $\xi_1 = (k_A + k_B)d$; $\xi_1 = (k_A - k_B)d$

The subscript "A" is used for AlN and "B" used for GaN

$$[Q_2][Q_1] = [Q]$$

$$= \frac{1}{\alpha^2 - \beta^2}\begin{bmatrix} \alpha^2 \exp(\xi_1) + \beta^2 \exp(\xi_2) & -\alpha\beta \exp(-\xi_2) - \alpha\beta \exp(-\xi_1) \\ -\alpha\beta \exp(\xi_1) - \alpha\beta \exp(\xi_2) & \alpha^2 \exp(-\xi_1) + \beta^2 \exp(-\xi_2) \end{bmatrix}$$

Let, $\qquad a = \frac{\alpha^2 \exp(\xi_1) + \beta^2 \exp(\xi_2)}{\alpha^2 - \beta^2} \qquad ; \qquad b = \frac{-\alpha\beta \exp(-\xi_2) - \alpha \exp(-\xi_1)}{\alpha^2 - \beta^2}$

$c = \frac{-\alpha\beta \exp(\xi_1) - \alpha \exp(\xi_2)}{\alpha^2 - \beta^2}; \quad d = \frac{\alpha^2 \exp(-\xi_1) + \beta^2 \exp(-\xi_2)}{\alpha^2 - \beta^2}$

Since, matrix multiplication is associative, we can write:

$$[C_9] = [Q_8][Q_7][Q]^3[Q_0][C_0]$$

$$\frac{X_{11}(a^2 b + b^2 c + abd + bd^2) + X_{12}(abc + 2bcd + d^3)}{X_{11}(a^3 + 2abc + bcd) + X_{12}(a^2 c + acd + bc^2 + d^2 c)} = -\frac{\varepsilon_A k_A + q}{\varepsilon_A k_A - q} \quad (63)$$

The above is the final dispersion relation, where:

$$X_{11} = \frac{(\varepsilon_B k_B + \varepsilon_A k_A)(\varepsilon_9 k_9 + \varepsilon_B k_B)exp\big((k_B + k_A)d\big) + (\varepsilon_B k_B - \varepsilon_A k_A)(\varepsilon_9 k_9 - \varepsilon_B k_B)exp\big((k_B - k_A)d\big)}{4\varepsilon_9 k_9 \varepsilon_B k_B}$$

$$X_{12} = \frac{(\varepsilon_B k_B + \varepsilon_A k_A)(\varepsilon_9 k_9 - \varepsilon_B k_B)exp\big((k_A - k_B)d\big) + (\varepsilon_B k_B - \varepsilon_A k_A)(\varepsilon_9 k_9 + \varepsilon_B k_B)exp(-(k_B + k_A)d)}{4\varepsilon_9 k_9 \varepsilon_B k_B}$$

In the present thesis the analysis has been restricted to finding the dispersion relation only for AlN/GaN superlattice; however nothing restricts one from applying Eq. 62 to get the amplitude of the Frohlich potential for the interface mode in the allowed frequency range.

CHAPTER 5 Determination of Frohlich Potential In MOS₂

5.1 Introduction

Graphene - a one atom thick two-dimensional material which is an allotrope of carbon - has some unique electrical properties such as zero electron effective mass, mobility as high as 15000 cm^2/V-s and zero band gap [27]. The principal factor limiting its application in electronic devices is its zero band gap which does not allow it to be used in logic circuits for low power switching applications [28]. Also, attempts to open a bandgap in graphene results in fabrication complexity and can lead to reduced mobility comparable to strained silicon films [29]. Due to these limitations of graphene, recent researches has been shifted to explore transition metal-dichalcogenide materials. TMDCs, whose generalized formula is MX2 (M = Transition metal (Pt, Pd, Ni, Ir, Rh, Co, Re, Tc, W, Mo, Ta, Nb, V, Hf, Zr and Ti), X = Chalcogen (Te, Se and S))[30]. These materials are also two-dimensional like graphene with a non-zero bandgap. The individual layers of these materials may be stacked one over the other to form the "bulk" material; every layer is separated from the adjacent layer by a van der Waals gap. MoS$_2$ belongs to transition metal-dichalcogenide group. One monolayer of MoS$_2$ has a band gap of 1.8 eV and is a direct gap semiconductor [30]

Phonons in MoS$_2$ exist in both in-plane and out-of-plane direction. The A$_2'$ (out-plane) mode and E' (in-plane) mode are infra-red active [31]. In this chapter we will derive the analytical expression for the Frohlich potential inside the 1-monolayer thick MoS$_2$ due to A$_2'$ (out-plane) mode vibration inspired by the results of Kaasbjerg et al. [32]and Sohier et al. [33]

5.2 Crystal Structure and Phonon Modes

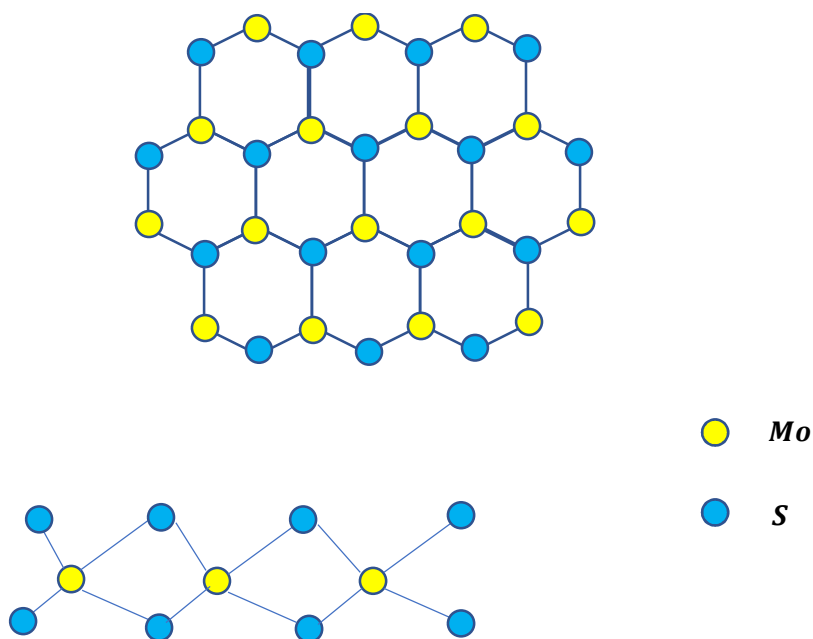The figure below shows 1-monolayer thick MoS_2.

● Mo

● S

Figure 34 One-monolayer thick MoS_2 crystal structure

As can be seen above that a 1-monolayer of MoS_2 has a sheet of Mo atoms sandwiched between two S atom sheets. MoS_2 has a honeycomb lattice structure.

Various phonon modes are shown in figure below for a 1-monolayer thick MoS_2:
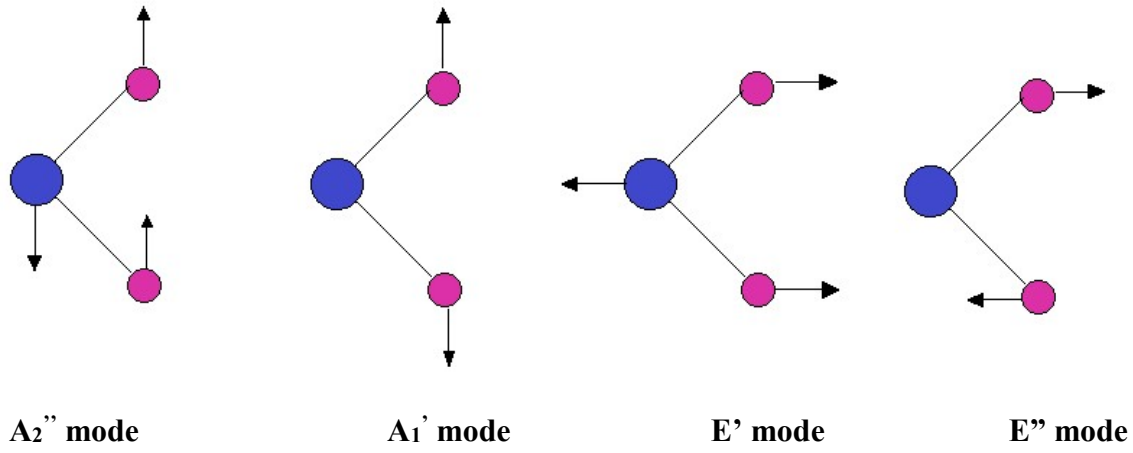
$A_2^{''}$ mode $A_1^{'}$ mode   E' mode   E" mode

Figure 35 Various phonon modes in 1-monoLayer MoS2.
$A_2^{''}$ and E' mode are IR active. Reference: Phy Rev B Vol 89, 035438 (2014)

5.3 $A_2^{'}$ mode Analysis

Consider for example a 3-layer MoS_2 as shown in Fig. 36, here it is observed that the vertical mode vibration as in $A_2^{''}$ mode propagates in the z-direction as wave due to which the individual atomic displacement is function of z and wavevector. But for a single monolayer case there is no z-dependence of the atoms in the vertical direction. In $A_2^{''}$ mode the Mo and S atoms vibrate out-of-phase with respect to each other. Our main objective is to find the polarization created per unit volume due to this out-of-phase vibration and then evaluating the resulting potential due to this polarization.
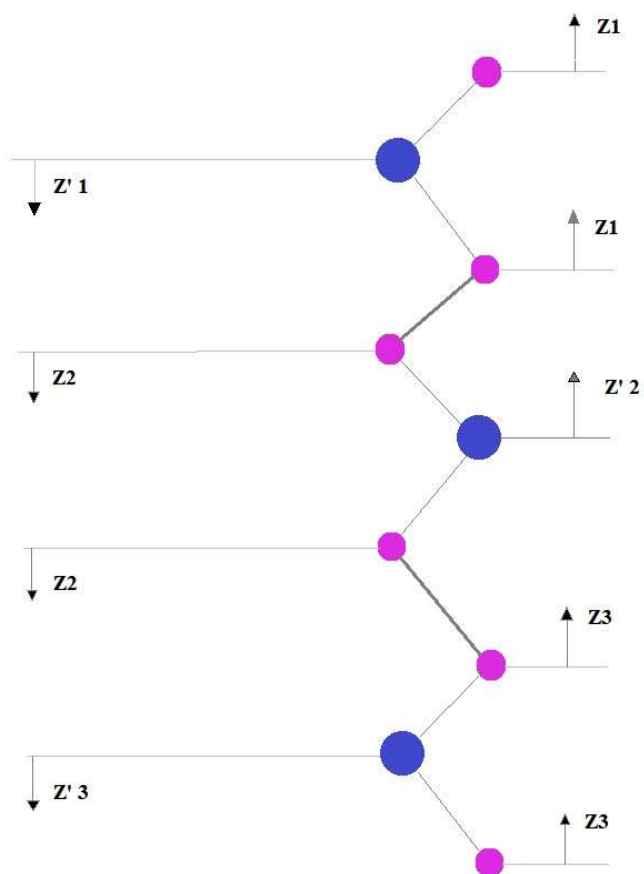
Figure 36 A2' mode in a 3-layer MoS2.

The big circles depict Mo atoms and the small ones depict S atoms. The thick lines between S atoms represents the van der Waals bonds

For 1-mono layer of MoS_2 the A2 mode of optical phonon is shown as under:
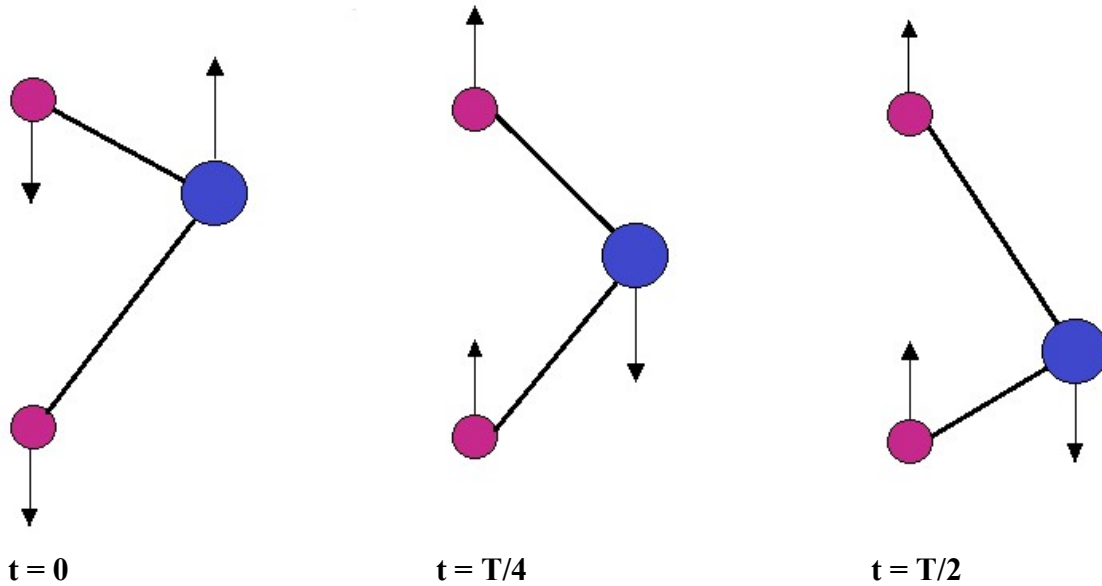

Figure 37 The vibration pattern of Mo and S in the unit cell of 1-monolayer thick MoS2 at different time instances

The Magenta colored atoms represent sulphur atoms while the blue color atom is molybdenum atom. Both atoms vibrate out of phase with respect to each other along the z-axis. For 1-monolayer of material the displacement of atoms has only sinusoidal dependence on time whereas there is no z-dependence because no wave is propagating for one monolayer.

The above figure shows the atomic positions for one-half cycle of vibration. As shown in the figure above, it will be assumed that at time $t = 0$ both Mo and S atoms are at their extrema positions and further continue their motion as per the Fig. 37.

<u>**Polarization calculation due to A$_2$' mode vibration pattern:**</u>

Let the amplitude of vibration of Mo and S atoms be **A, so the displacement of atom at any**

instant of time is: A$e^{-i\omega t}$. Thus the net dipole moment can be written as : **Z* (4A).** The figure

below clarifies the net dipole moment expression so obtained:
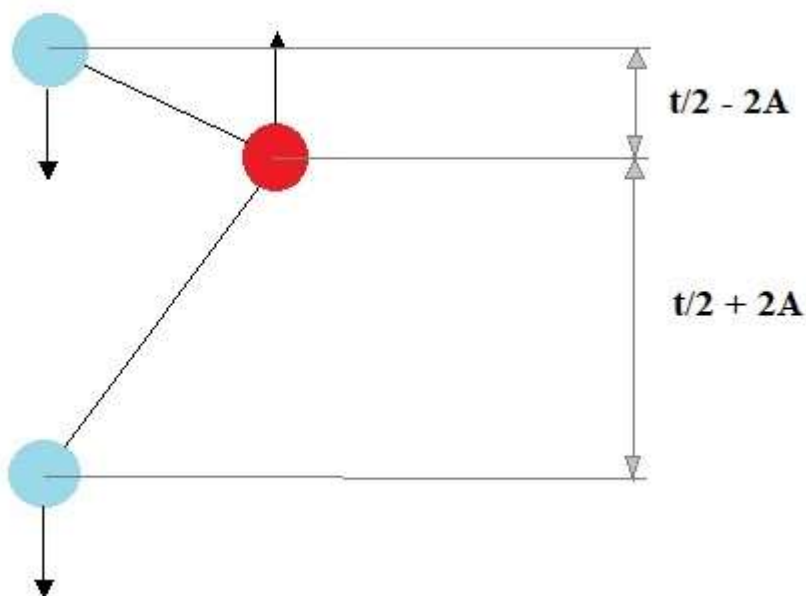
Mo and S atoms at one extremum of their Vibration

Figure 38 The initial position of Mo and S atoms starting from their extremum

Net dipole moment: Z* (t/2 -2A)- Z* (t/2+2A) = Z*(4A)

(N.B.: The time dependence have been suppressed in all of the expressions.)

Polarization: Net dipole moment per unit volume $= \dfrac{Z^* 4A \, f(z)}{\epsilon_\infty S} \, \hat{e}_z$ (64)

In the above expression **S** represents the area

Now by Poisson's equation, we have:

$$\nabla^2 \varphi(z) = -\frac{\rho}{\epsilon_\infty} = -\frac{\nabla.P}{\epsilon_\infty} \tag{65}$$

Since, $\nabla \equiv \dfrac{\partial}{\partial q} \, \hat{e}_q + \dfrac{\partial}{\partial z} \, \hat{e}_z \Rightarrow \nabla.P = \dfrac{Z^* 4A}{\epsilon_\infty S} \, \dfrac{\partial f(z)}{\partial z}$ (66)

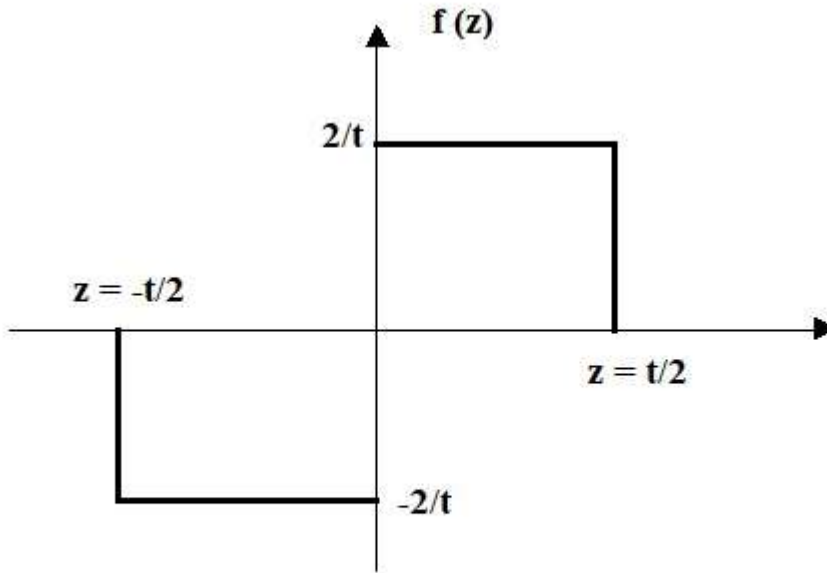Now, f(z) represents the profile of polarization in the z-direction given below in the figure

Figure 39 Polarisation profile in 1-Monolayer thick MoS$_2$

Taking the Fourier transform of the poisons equation we have:

$$(q^2 + k^2)\varphi_q(k) = -\frac{Z^*}{\epsilon_\infty S}(4A)\mathcal{F}\left(\frac{\partial f(z)}{\partial z}\right)$$

Here, $\mathcal{F}\left(\frac{\partial f(z)}{\partial z}\right)$ denotes the fourier transform of $\frac{\partial f(z)}{\partial z}$

The Fourier transform of $\frac{\partial f(z)}{\partial z} = ik\,\mathcal{F}(f(z)) = ik\left(\frac{2}{ik} - \frac{2\,sin(ka)}{k} - 2\pi\delta(k)\right)$

$$= \frac{2}{t}\left(2 - 2i\,sin\left(k\frac{t}{2}\right) - 2\pi ik\delta(k)\right)$$

Note: $\delta(k) = unit\ impulse\ function$

Substituting the above expression in the Fourier transform equation of Poisson's equation:

$$\varphi_q(k) = \frac{Z^*4A\left(2 - 2i\,sin\left(k\frac{t}{2}\right) - 2\pi ik\delta(k)\right)}{\epsilon_\infty S(q^2 + k^2)} \qquad (67)$$

Now, we will take inverse Fourier transform of the above expression to get $\varphi_q(z)$, as shown below:

$$\varphi_q(z) = \int_{-\infty}^{+\infty} dk\, e^{ikz}\, \varphi_q(k) \qquad (68)$$

Thus,

$$\varphi_q(z) = \frac{Z^*4A}{\epsilon_\infty S}\frac{2}{t} \int_{-\infty}^{+\infty} dk\, e^{ikz}\, \frac{\left(2 - 2i\,sin\left(k\frac{t}{2}\right) - 2\pi i k\delta(k)\right)}{(q^2 + k^2)}$$

$$= \frac{Z^*8A}{q\epsilon_\infty St}\int_{-\infty}^{+\infty} dk\, e^{ikz}\, \frac{2q}{(q^2+k^2)} - \frac{Z^*8A}{2q\epsilon_\infty St}\int_{-\infty}^{+\infty} dk\, e^{ik\left(z+\frac{t}{2}\right)}\, \frac{2q}{(q^2+k^2)} +$$

$$\frac{Z^*8A}{2q\epsilon_\infty St}\int_{-\infty}^{+\infty} dk\, e^{ik\left(z-\frac{t}{2}\right)}\, \frac{2q}{(q^2+k^2)}$$

$$= \frac{Z^*8A}{q\epsilon_\infty St} e^{-q|z|} - \frac{Z^*8A}{2q\epsilon_\infty St} e^{-q\left|z+\frac{t}{2}\right|} + \frac{Z^*8A}{2q\epsilon_\infty St} e^{-q\left|z-\frac{t}{2}\right|}$$

Thus,

$$\varphi_q(z) = \frac{Z^*8A}{q\epsilon_\infty St} e^{-q|z|} - \frac{Z^*4A}{q\epsilon_\infty St} e^{-q\left|z+\frac{t}{2}\right|} + \frac{Z^*4A}{q\epsilon_\infty St} e^{-q\left|z-\frac{t}{2}\right|} \qquad (69)$$

The above is the expression for the Frohlich potential as a function of z-direction for A₂' Mode

Note: For simplicity of expression, let $\dfrac{t}{2} = \boldsymbol{a}$

The region of 1-mono layer MoS$_2$ can be classified as below:

$$0 \leq z \leq +a$$
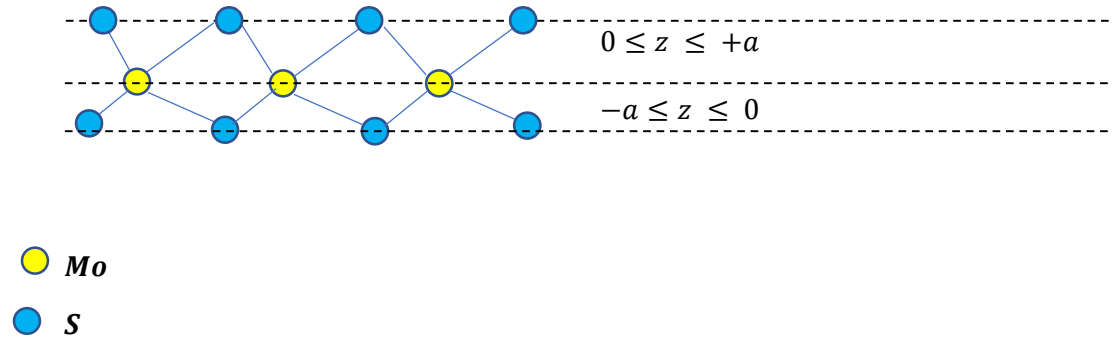$$-a \leq z \leq 0$$

○ **Mo**

○ **S**

Figure 40 1-ML thick MoS2 with region markings used in determination of potential

The region wise breakup of expression of interaction potential so obtained as above can be written as:

$$\varphi_q(z) = \begin{cases} \dfrac{Z^*(8A)}{\epsilon_\infty St} \cdot \dfrac{1}{q} \cdot \left(e^{-qz} + e^{-qa}\,sinh(qz)\right), & z > 0 \\[4mm] \dfrac{Z^*(8A)}{\epsilon_\infty St} \cdot \dfrac{1}{q} \cdot \left(e^{qz} + e^{-qa}\,sinh(qz)\right), & z < 0 \end{cases}$$
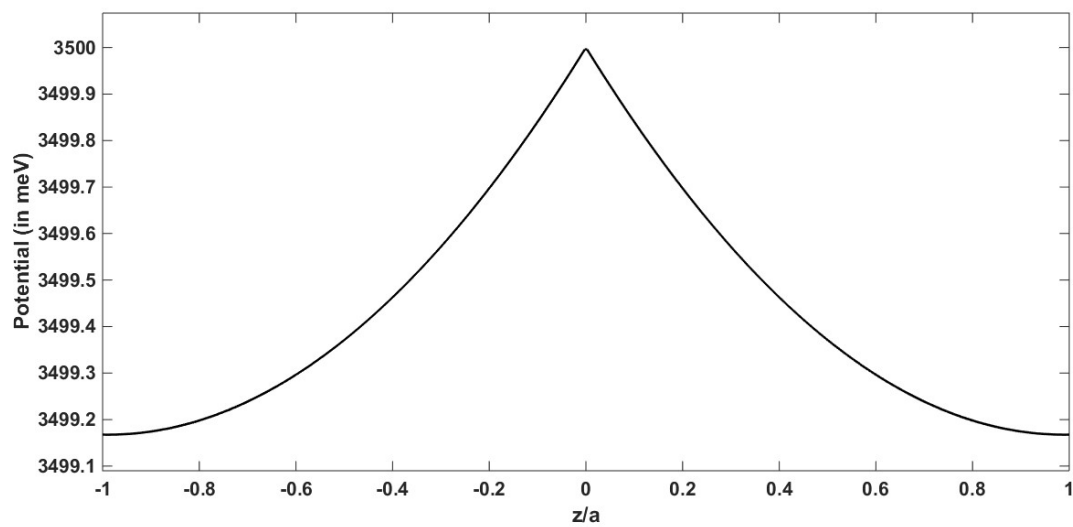
In the above analysis t = 2a = 0.441 nm [32]

(70)

Figure 41 Potential inside 1-ML MoS2 as function of z for q = 0.1
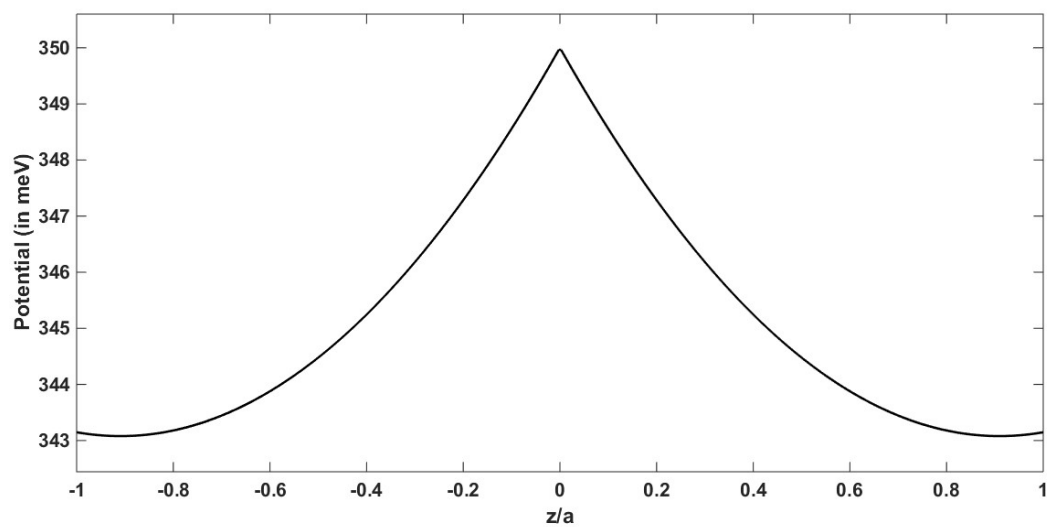

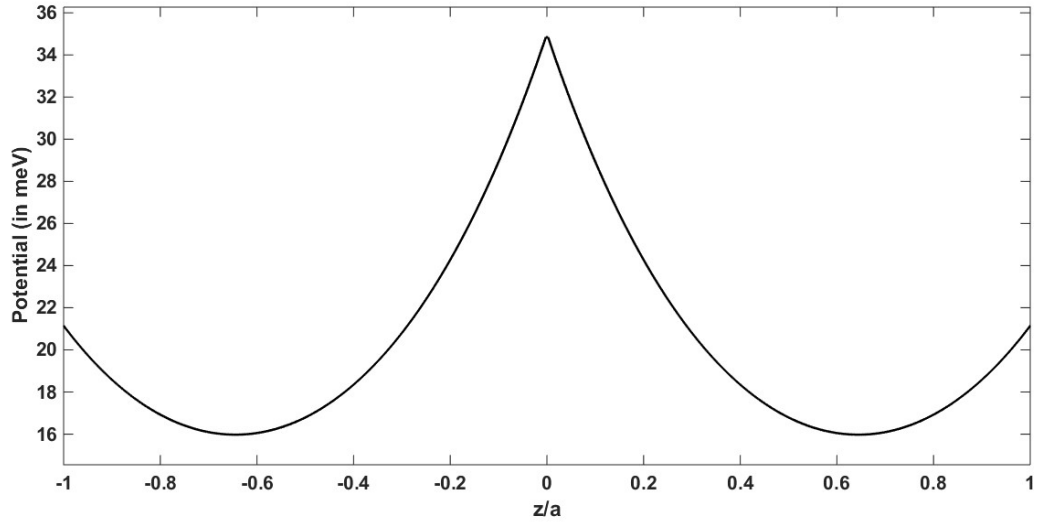**Figure 42** Potential inside 1-ML MoS2 as function of z for q = 1

Figure 43 Potential inside 1-ML MoS2 as function of z for q = 10
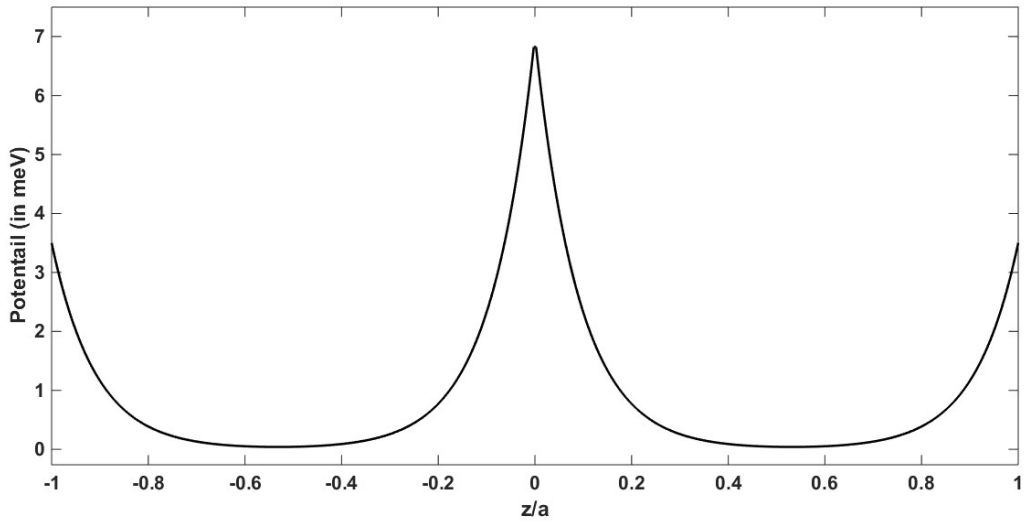

Figure 44 Potential inside 1-ML MoS2 as function of z for q = 50

The following conclusions can be drawn from the above graphs:

1. The Frohlich potential inside the MoS$_2$ layer depends on the in-plane phonon wavevector q

2. The potential has 1/q dependence – As q → 0 the potential becomes very high (3.5 eV near middle of the layer). The short wavelength in-plane phonon, for example. q = 50 have very low (7meV) potential in the middle of the layer.

3. For short wavelength (large q) in-plane phonons the potential inside the layer decreases at a very steep rate and the difference between the potential at the middle of the layer to the potential at the edge of the layer is very high as compared to long wavelength (q → 0) in-plane phonons.

Evaluation of Coupling Function g_{LO}

The phonon-electron coupling function, g_{LO}, is defined as :

$$g_{LO} = \int dz \, \chi^*(z) \, \varphi_q(z)\chi(z) \qquad (71)$$

In the above expression $\chi(z)$ is the **electron envelope function**

For bulk material $g_{LO} = \frac{1}{q} \sqrt{\frac{e^2\hbar\omega_{LO}}{2\varepsilon_0 V}} \left(\frac{1}{\varepsilon(\infty)} - \frac{1}{\varepsilon(0)}\right)^{1/2}$

The expression of $\chi(z)$ is taken as double bell gaussian shape curve for MoS$_2$. The two bells are centered around z= -a and z = +a

$$\chi(z) = \frac{1}{\pi^{\frac{1}{4}}\sqrt{\sigma}} \left(e^{-(z-a)^2/2\sigma^2} + e^{-(z+a)^2/2\sigma^2} \right) \qquad (72)$$

Fig 45 shows the plot of electron envelope function:

Evaluation of g_{LO} for 0< z< +a:

$$=$$

$$\frac{Z^*(8A)}{\epsilon_\infty St}\cdot\frac{1}{q}\cdot\frac{1}{\sqrt{\pi}\sigma}\int_0^a dz\ (e^{-qz}+e^{-qa}\sinh(qz))\left(e^{-(z-a)^2/\sigma^2}+e^{-(z+a)^2/\sigma^2}+2\,e^{-(z^2+a^2)/\sigma^2}\right)$$

$$=$$

$$\frac{Z^*(8A)}{\epsilon_\infty St}\cdot\frac{1}{q}\left(e^{\frac{q^2\sigma^2}{4}}\left(erf\left(\frac{q\sigma}{2}\right)-erf\left(\frac{q\sigma}{2}-\frac{a}{\sigma}\right)\right)\left(e^{-qa}-\frac{1}{2}\right)\right.$$

$$+\frac{e^{\frac{q^2\sigma^2}{4}}}{4}\left(erf\left(\frac{a}{\sigma}+\frac{q\sigma}{2}\right)-erf\left(\frac{q\sigma}{2}\right)\right)$$

$$+\frac{e^{\frac{q^2\sigma^2}{4}+qa}}{2}\left(erf\left(\frac{2a}{\sigma}+\frac{q\sigma}{2}\right)-erf\left(\frac{a}{\sigma}+\frac{q\sigma}{2}\right)\right)$$

$$+\frac{e^{\frac{q^2\sigma^2}{4}-2qa}}{4}\left(erf\left(\frac{2a}{\sigma}-\frac{q\sigma}{2}\right)-erf\left(\frac{a}{\sigma}-\frac{q\sigma}{2}\right)\right)$$

$$-\frac{e^{\frac{q^2\sigma^2}{4}}}{4}\left(erf\left(\frac{2a}{\sigma}+\frac{q\sigma}{2}\right)-erf\left(\frac{a}{\sigma}+\frac{q\sigma}{2}\right)\right)$$

$$+e^{\left(\frac{q^2\sigma^2}{4}-\frac{a^2}{\sigma^2}\right)}\left(erf\left(\frac{a}{\sigma}+\frac{q\sigma}{2}\right)-erf\left(\frac{q\sigma}{2}\right)\right)$$

$$+e^{\left(\frac{q^2\sigma^2}{4}-\frac{a^2}{\sigma^2}-qa\right)}\left(erf\left(\frac{a}{\sigma}-\frac{q\sigma}{2}\right)+erf\left(\frac{q\sigma}{2}\right)\right)$$

$$\left.-e^{\left(\frac{q^2\sigma^2}{4}-\frac{a^2}{\sigma^2}-qa\right)}\left(erf\left(\frac{a}{\sigma}+\frac{q\sigma}{2}\right)+erf\left(\frac{q\sigma}{2}\right)\right)\right)\quad(73)$$

Evaluation of g_{LO} for -a< z< 0:

$$= $$

$$\frac{Z^*(8A)}{\epsilon_\infty St} \cdot \frac{1}{q} \cdot \frac{1}{\sqrt{\pi}\sigma} \int_{-a}^{0} dz \left(e^{qz} + e^{-qa} \sinh(qz) \right) \left(e^{-(z-a)^2/\sigma^2} + e^{-(z+a)^2/\sigma^2} + 2\, e^{-(z^2+a^2)/\sigma^2} \right)$$

Substituting z= - x in the above expression we have:

$$\frac{Z^*(8A)}{\epsilon_\infty St} \cdot \frac{1}{q} \cdot \frac{1}{\sqrt{\pi}\sigma} \int_{0}^{a} dz \left(e^{-qx} - e^{-qa} \sinh(qx) \right) \left(e^{-(x-a)^2/\sigma^2} + e^{-(x+a)^2/\sigma^2} + 2\, e^{-(x^2+a^2)/\sigma^2} \right)$$

It is observed that the above expression is same as that for 0<z< +a case except for "minus" sign before sinh (qx)

Consequently, the above integral is evaluated as below:

$$\frac{Z^*(8A)}{\epsilon_\infty St}\cdot\frac{1}{q}\left(e^{\frac{q^2\sigma^2}{4}}\left(erf\left(\frac{q\sigma}{2}\right)-erf\left(\frac{q\sigma}{2}-\frac{a}{\sigma}\right)\right)\left(e^{-qa}-\frac{1}{2}\right)+\frac{e^{\frac{q^2\sigma^2}{4}}}{4}\left(erf\left(\frac{a}{\sigma}+\frac{q\sigma}{2}\right)-erf\left(\frac{q\sigma}{2}\right)\right)-\right.$$

$$\frac{e^{\frac{q^2\sigma^2}{4}+qa}}{2}\left(erf\left(\frac{2a}{\sigma}+\frac{q\sigma}{2}\right)-erf\left(\frac{a}{\sigma}+\frac{q\sigma}{2}\right)\right)-\frac{e^{\frac{q^2\sigma^2}{4}-2qa}}{4}\left(erf\left(\frac{2a}{\sigma}-\frac{q\sigma}{2}\right)-erf\left(\frac{a}{\sigma}-\frac{q\sigma}{2}\right)\right)+$$

$$\frac{e^{\frac{q^2\sigma^2}{4}}}{4}\left(erf\left(\frac{2a}{\sigma}+\frac{q\sigma}{2}\right)-erf\left(\frac{a}{\sigma}+\frac{q\sigma}{2}\right)\right)-e^{\left(\frac{q^2\sigma^2}{4}-\frac{a^2}{\sigma^2}\right)}\left(erf\left(\frac{a}{\sigma}+\frac{q\sigma}{2}\right)-erf\left(\frac{q\sigma}{2}\right)\right)-$$

$$\left.e^{\left(\frac{q^2\sigma^2}{4}-\frac{a^2}{\sigma^2}-qa\right)}\left(erf\left(\frac{a}{\sigma}-\frac{q\sigma}{2}\right)+erf\left(\frac{q\sigma}{2}\right)\right)+e^{\left(\frac{q^2\sigma^2}{4}-\frac{a^2}{\sigma^2}-qa\right)}\left(erf\left(\frac{a}{\sigma}+\frac{q\sigma}{2}\right)+erf\left(\frac{q\sigma}{2}\right)\right)\right)$$
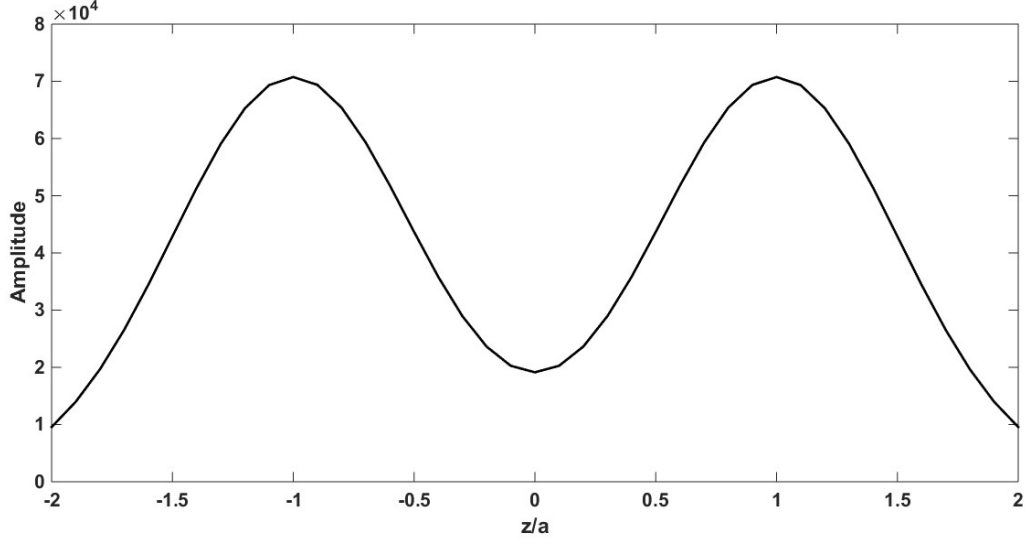
$$(74)$$

Figure 45 Electron envelope function in MoS2

For the above "double-bell" electron envelope function $\sigma = a/2$ has been assumed.

5.4 Conclusions

In this chapter we have presented a detailed mathematical analysis to find the electron-interaction potential due to out-of-plane (A_2' mode phonon) vibration of Mo and S atoms. Also, we extended the calculation to find the coupling function for 1-monolayer MoS_2, the coupling function is an important determinant in finding the scattering rate of electrons by phonons. The major conclusions drawn can be summarized as:

1. For 1-monolayer MoS_2, the potential induced by out-of-plane vibration has no dependence on spatial co-ordinate (z-direction in the present case).

2. The potential as obtained above (A_2' phonon mode) depends on the in-plane phonon wavevector.

3. The A_2' phonon mode potential has very high amplitude at the middle of the layer and then exponentially decreases on either sides.

4. Only for a long wavelength in-plane phonon wavevector do we observe very high potential, e.g., 3.5 eV for q = 0.1 at the middle of the layer, whereas for short wavelength in-plane phonons we get 7 meV for q = 50.

5. It can be concluded that the long wavelength phonons play the most significant role in electron scattering.

PUBLICATIONS AND PRESENTATIONS IN PROGRESS

1. Michael A. Stroscio, Mitra Dutta, Ramji Singh, Mojgan Mazouchi, Debopam Datta, Ahmed Mohamad, Ketaki Sarkar, Ke (Clare) Sun, Arash Darbandi, Kihoon Park, Can Bayram, Continuum Models of Phonons in Nanostructures: Confined Phonon Effects in Heterostructure Devices, AFRL, July 2, 2018.

2. Michael A. Stroscio, Mitra Dutta, Ramji Singh, Mojgan Mazouchi, Debopam Datta, Ahmed Mohamad, Ketaki Sarkar, Ke (Clare) Sun, Arash Darbandi, Kihoon Park, Can Bayram, Continuum Models of Phonons in Nanostructures: Confined Phonon Effects in Heterostructure Devices with Specifics for 2D Materials, Workshop on 2D Materials, UIC CoE and LAS, hosted by Chemical Engineering, July 17, 2018.

3. Mitra Dutta, Michael A. Stroscio, Ramji Singh, and Toan Pham, Understanding Phonon Effects in 2D/3D Structures: Continuum Models of Phonons in Nanostructures, Army Research Laboratory, Adelphi, MD, August 24, 2018.

4. Ramji Singh, Mitra Dutta, and Michael Stroscio, University of Illinois, Chicago, Optical Phonons in 2D-3D Structures: Dispersion Relations and Frohlich Potentials, WOCSEMADD 2019, February 18, 2019; the UIC research on these 2D structures is being written up for a separate journal publication.

5. Ramji Singh, M Dutta, M Stroscio and AG Birdwell and Paul M Amritharaj Interface-phonon — electron Interaction Potentials and Dispersions Relations in III-nitride-based structures, submitted to the *Journal of Applied Physics*.

REFERENCES

1. M. A. Stroscio and M. Dutta, Phonons in Nanostructures (Cambridge University Press, Cambridge, 2001)

2. I.K Oh, Jai Singh, A. Thilagam and A.S. Vengurlekar, Physical Review B, 62 pp. 2045 (2000)

3. P. Vogl, Physics of nonlinear transport in semiconductor, Proceedings of the NATO Advanced Study (Plenum, NY, 1980)

4. Michael A. Stroscio, Journal of Applied Physics, 80, 6864 (1996).

5. SeGi Yu, K. W. Kim, Michael A. Stroscio, G. J. Iafrate, J.-P. Sun, and G. I. Haddad, Journal of Applied Physics, 82, 3363 (1997).

6. H. B. Teng, J. P. Sun, G. I. Haddad, M. A. Stroscio, S. Yu, and K. W. Kim, J. Appl. Phys, 84, 2155 (1998).

7. Mikhail V. Kisin, Michael A. Stroscio, Gregory Belenky, Vera B. Gorfinkel, and Serge Luryi, J. Appl. Phys., 83 4816 (1998)

8.. Mikhail V. Kisin, Michael A. Stroscio, Gregory Belenky, Vera B. Gorfinkel, and Serge Luryi, Journal. Appl. Phys., 83 4816 (1998); Michael A. Stroscio, Mikhail V. Kisin, Gregory Belenky, and Serge Luryi, Phonon Enhanced Inverse Population in Asymmetric Double Quantum Wells, Applied Physics Letters, 75, 3258 (1999).

9. B. S. Williams, B. Xu, Q. Hu, Applied Physics Letters, 75, 2927 (1999).

10. V. M. Menon, L. R. Ram-Mohan, W. D. Goodhue, A. J. Gatesman, A. S. Karakashian,, Physica B, 316-317, 212-215 (2002).

11. V. Spagnolo, G. Scamarcio, M. Troccoli, F, Capasso, C. Gmachl, A. M. Sergent, A. L. Hutcheson, D. L. Sivco, and A. Y. Cho, Applied Physics Letters, 80, 4303-4305 (2002).

12. B. C. Lee, K. W. Kim, M. Dutta and M. A. Stroscio, Phys. Rev., B56, 997 (1997).

13. B. C. Lee, K.W. Kim, M. A. Stroscio and M. Dutta, Phys. Rev. B, 58, 4860 (1998).

14. S. M. Komirenko, K. W. Kim, M. A. Stroscio and M. Dutta, Phys. Rev. B, 59, 5013 (1999)

15. S. M. Komirenko, K. W. Kim, M. A. Stroscio and M. Dutta, Phys. Rev. B, 61, 2034 (2000)

16. J. Gleize, M. A. Renucci, J. Frandon and F. Demangeot, Phys. Rev, B, 60, 15985 (1999).

17. C. F. Lin, H. C. Cheng, J. A. Huang, M. S. Feng, J. D. Guo, and G. C. Chi, Appl. Phys. Lett. 70, 2583 (1997).

REFERENCES (continued)

18. R. Gaska, Q. Chen, J. Yang, A. Osinsky, M. Asif Khan, and M. S. Shur, IEEE Electron Device Lett. 18, 492 (1997).

19. Chen Chen, Mitra Dutta, and Michael A. Stroscio, Journal of Applied Physics, 95, 2540-2546 (2004).

20. Chen Chen, Mitra Dutta, and Michael A. Stroscio, Phys. Rev., B70, 075316-1-7, 2004.

21. N. Zhang, Sicheng Laio, M. Dutta and M. A. Stroscio, Journal of Applied Physics, 114, 054312 (2013) on line August 6, 2013: doi: 10.1063/1.4817528

22. N. Zhang, M. Dutta and M. A. Stroscio, Solid State Electronics, 94, 72-81 (2014).

23. K. Park, M. A. Stroscio, and C. Bayram, Journal of Applied Physics, 121(24), 245109-1-8 (2017).

24. Kihoon Park, Ahmed Mohamad, Can Bayram, Mitra Dutta, and Michael A. Stroscio, Nature Scienific Reports, 8, 15947 (2018).

25. Terrence P. O'Regan, Dmitry Ruzmetov, Mahesh R. Neupane, Robert A. Burke, Andrew A. Herzing, Kehao Zhang, A. Glen Birdwell, DeCarlos E. Taylor, Edward F. C. Byrd, Scott D. Walck, Albert V. Davydov, Joshua A. Robinson, and Tony G. Ivanov, APL, 111, 051602 (2017).

26. Dmitry Ruzmetov, Kehao Zhang, Gheorghe Stan, Berc Kalanyan, Ganesh R. Bhimanapati, Sarah M. Eichfeld, Robert A. Burke, Pankaj B. Shah, Terrance P. O'Regan, Frank J. Crowne, A. Glen Birdwell, Joshua A. Robinson, Albert V. Davydov, and Tony G. Ivanov, Vertical 2D/3D Semiconductor Heterostructures Based on Epitaxial Molybdenum Disulfide and Gallium Nitride, ACS Nano, 10, 3580-3588 (2016).

27. Geim, A.K; Novoselov, K.S (2007) "The Rise of Graphene". Nature Maerials 6 (3).

28. Novoselov KS, Geim AK, Morozov SV, Jiang D, Zhang Y, Dubonos SV, et al. Electric field effect in atomically thin carbon films. Science 2004.

29. B. Radisavljevic, A. Radenovic, J. Brivio, V. Giacometti and A. Kis, Nature Nanotechnology, 6 (2011), 147-150

30. Xiao Li, Hongwei Zhu, Journal of Materionomics (2015), 33-44

31. Yongqing Cai, Jinghua Lan, Gang Zhang, and Yong-Wei Zhang Phy Rev B Vol 89, 035438 (2014)

32. Kristen Kaasbjerg, Kristan S. Thygesen and Karsten W. Jacobsen Phys. Rev. B 85, 115317 (2012)

REFERENCES (continued)

33. Thibault Sohier, Matteo Calandra, and Francesco Mauri Phys. Rev. B **94**, 085415

34. Yu, Kim, Bergman, Dutta, Stroscio and Zavada, Phys. Rev. B **58**, 15283 (1998)

35. Yu, Kim, Stroscio, lafrate, Sun and Haddad Journal of Applied Physics **82**, 3363 (1997)

VITA

NAME: Ramji Singh

EDUCATION: B.TECH., Electronics and Communication Engineering, Saroj Institute of
                  Technology and Management, Uttar Pradesh Technical University,
                  Lucknow, India, 2005

                  M.S., Electrical and Computer Engineering, University of Illinois at
                  Chicago, Chicago, Illinois, 2019

WORK: 1. Teaching Assistant, UIC Spring 18 & Fall 18
                  2. Research Assistant, UIC Summer18, Fall 18 & Spring 19

HONORS: Tuition Fee Waiver, University of Illinois at Chicago, Spring 18, Fall 18
                  and Spring 19